Article

Current Biology

Unusual morphology in the mid-Cretaceous lizard *Oculudentavis*

Highlights

- A new species of the reptile in amber, *Oculudentavis*, is described
- *Oculudentavis* is a bizarre lizard, not a bird
- The bird-like appearance of *Oculudentavis* is due to convergence in skull proportions

Authors

Arnau Bolet, Edward L. Stanley, Juan D. Daza, ..., Joseph J. Bevitt, Adolf Peretti, Susan E. Evans

Correspondence

juand.daza@gmail.com

In brief

Bolet et al. describe a second, more complete, specimen of the mid-Cretaceous genus *Oculudentavis* (new species) from the amber deposits of Myanmar. Comparative morphology and phylogenetic analyses prove that, despite its bird-like appearance, *Oculudentavis* is a bizarre lizard of uncertain affinities.

Bolet et al., 2021, Current Biology *31*, 1–12
August 9, 2021
https://doi.org/10.1016/j.cub.2021.05.040

CellPress

Please cite this article in press as: Bolet et al., Unusual morphology in the mid-Cretaceous lizard *Oculudentavis*, Current Biology (2021), https://doi.org/10.1016/j.cub.2021.05.040

Current Biology

CellPress
OPEN ACCESS

Article

Unusual morphology in the mid-Cretaceous lizard *Oculudentavis*

Arnau Bolet,[1,2] Edward L. Stanley,[3,14] Juan D. Daza,[4,12,13,*] J. Salvador Arias,[5] Andrej Čerňanský,[6] Marta Vidal-García,[7] Aaron M. Bauer,[8] Joseph J. Bevitt,[9] Adolf Peretti,[10] and Susan E. Evans[11]

[1]Institut Català de Paleontologia Miquel Crusafont, Universitat Autònoma de Barcelona, Barcelona, Spain
[2]School of Earth Sciences, University of Bristol, Bristol, UK
[3]Department of Natural History, Florida Museum of Natural History, Gainesville, FL, USA
[4]Department of Biological Sciences, Sam Houston State University, Huntsville, TX, USA
[5]Unidad Ejecutora Lillo (CONICET - Fundación Miguel Lillo), San Miguel, de Tucumán, Tucumán, Argentina
[6]Department of Ecology, Laboratory of Evolutionary Biology, Faculty of Natural Sciences, Comenius University in Bratislava, Bratislava, Slovakia
[7]Department of Cell Biology & Anatomy, University of Calgary, Calgary, AB, Canada
[8]Department of Biology and Center for Biodiversity and Ecosystem Stewardship, Villanova University, Villanova, PA, USA
[9]Australian Centre for Neutron Scattering, Australian Nuclear Science and Technology Organisation, Sydney, NSW, Australia
[10]GRS Gemresearch Swisslab AG and Peretti Museum Foundation, Meggen, Switzerland
[11]Department of Cell and Developmental Biology, University College London, London, UK
[12]Twitter: @Juan_Gecko
[13]Lead contact
[14]Twitter: @DrScanley
*Correspondence: juand.daza@gmail.com
https://doi.org/10.1016/j.cub.2021.05.040

SUMMARY

Oculudentavis khaungraae was described based on a tiny skull trapped in amber. The slender tapering rostrum with retracted narial openings, large eyes, and short vaulted braincase led to its identification as the smallest avian dinosaur on record, comparable to the smallest living hummingbirds. Despite its bird-like appearance, *Oculudentavis* showed several features inconsistent with its original phylogenetic placement. Here, we describe a more complete specimen that demonstrates *Oculudentavis* is actually a bizarre lizard of uncertain position. The new specimen is described as a new species within the genus *Oculudentavis*. The new interpretation and phylogenetic placement highlight a rare case of convergent evolution in skull proportions but apparently not in morphological characters. Our results re-affirm the importance of Myanmar amber in yielding unusual taxa from a forest ecosystem rarely represented in the fossil record.

INTRODUCTION

In a recent paper, Xing et al.[1] described a tiny skull (Hupoge Amber Museum, HPG-15-3) from amber deposits in northwestern Myanmar. The skull, the holotype of a new genus and species *Oculudentavis khaungraae*, has a long tapering rostrum with retracted narial openings, a long-toothed mandible with a short symphysis, a large eye supported by prominent scleral ring, an unpaired median frontal, and a triradiate postorbital. The broad, rather rounded, parietal lacks a parietal foramen and has supratemporal processes that descend vertically to meet short quadrates with well-developed lateral concavities. Xing et al.[1] coded the characters of *Oculudentavis* into a Mesozoic avian data matrix[2] and found it to be a stem-avian, one node crownward of the Jurassic *Archaeopteryx.*

GRS-Ref-28627 is a second Myanmar amber specimen preserving a skull of smaller size to that of HPG-15-3 and a partial postcranial skeleton (Figures 1, 2A–2J, and S1). Like the holotype of *Oculudentavis*, it has a long rostrum, a large orbit, a short postorbital region, and a long-toothed mandible. Although there are some proportional differences between the skulls as preserved, the anatomical features of individual bones strongly indicate that GRS-Ref-28627 is attributable to the genus *Oculudentavis* (Figures 2 and 3) but represents a different species. Moreover, many of its characters are in conflict with the interpretation of *Oculudentavis* as a stem bird. Instead, the characters indicate that *Oculudentavis* is a lizard, albeit a highly unusual one.

The interpretation of HPG-15-3 as a lizard rather than a bird has already been made; one metanalysis discussed its phylogenetic placement using an *ad hoc* revision of diagnostic features of diapsid clades but without testing the position of *Oculudentavis* in a phylogenetic analysis.[3] In a subsequent version of the paper, their hypothesis was tested and confirmed using an amniote data matrix[3] but with very limited sampling of squamates. In response to the first critique,[3] the original authors added

Please cite this article in press as: Bolet et al., Unusual morphology in the mid-Cretaceous lizard *Oculudentavis*, Current Biology (2021), https://doi.org/10.1016/j.cub.2021.05.040

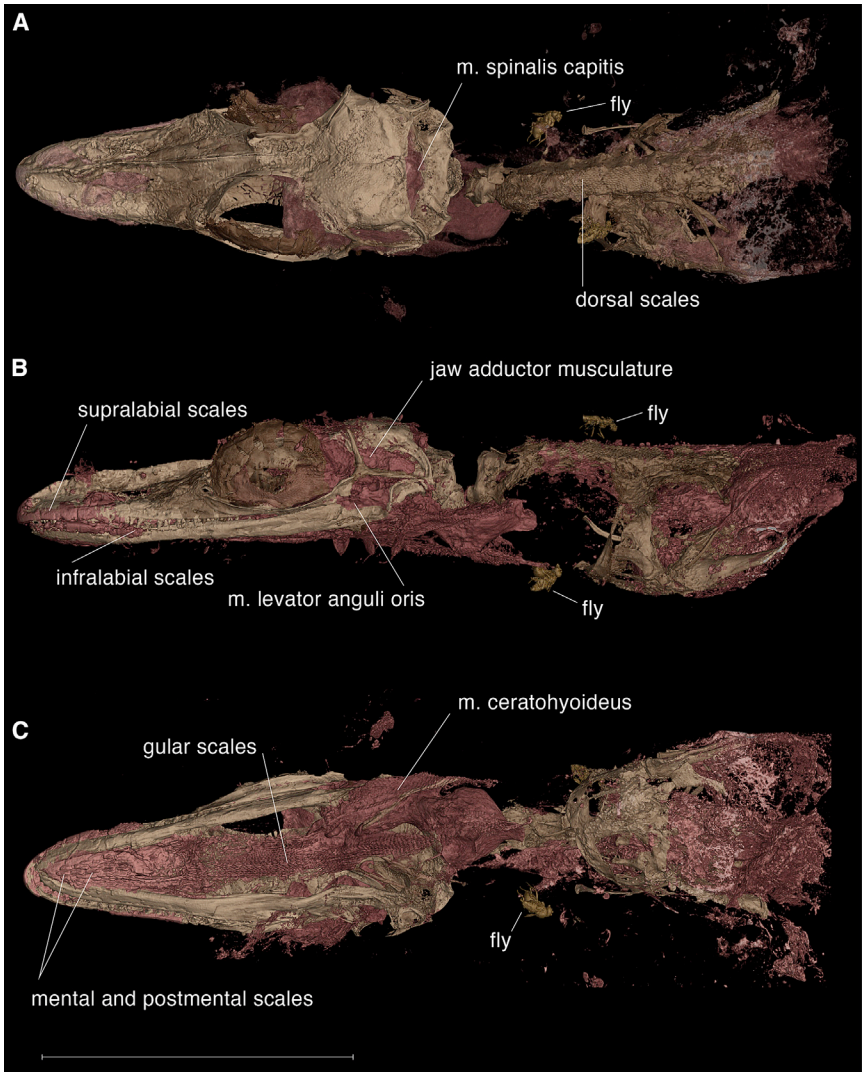

Figure 1. *Oculudentavis naga* (GRS-Ref-286278) displaying the superb preservation of bone and soft tissue

(A) Dorsal; (B) lateral; (C) ventral views. Scale bar represents 10 mm. Diptera associated with the lizard skeleton were identified as Phoridae, Platypezidae, Ceratopogonidae, or Brachycera (Empidoidea). See also Figures S1–S7 and Data S1.

Oculudentavis to an amniote dataset[4] and recovered *Oculudentavis* as well nested among a group of enantiornithine birds,[5] arguing that placement of this taxon with squamates only occurs if all avian taxa are removed. Herein, the phylogenetic allocation of *Oculudentavis* is tested in rigorous phylogenetic analyses using data derived from the holotype of *O. khaungraae* (HPG-15-3) and additional data from the new specimen (GRS-Ref-28627). Our analyses of an amniote dataset[6] with some additional taxa scored by us recovered *Oculudentavis* as a squamate reptile and not as a bird. We then explored the relationships of *Oculudentavis* within lizards using a comprehensive squamate dataset[7] with additional taxa (STAR Methods). In this paper, we correct the original description of this taxon and explore the amniote morphological dataset to determine whether convergent evolution of the skull of *Oculudentavis* with that of birds is supported by specific morphological characters. Additionally, both specimens were segmented digitally to provide a detailed description of the individual bones and to understand better the similarities and differences between them. The two specimens were also compared using retrodeformation methods. Based on this information, we provisionally place GRS-Ref-28627 in a new species. If new specimens are recovered in the future, they may help to determine whether the observed differences represent interspecific variation, intraspecific variation, or preservational artifact.

RESULTS

Systematic paleontology

Reptilia Laurenti, 1768
Lepidosauromorpha Benton, 1983
Squamata Oppel, 1811
Genus *Oculudentavis* Xing et al.[1]
Type species *Oculudentavis khaungraae* Xing et al.[1]

Note: The retraction[8] of the original description of this taxon[1] does not affect the nomenclatural availability of *Oculudentavis khaungraae* under the International Code of Zoological Nomenclature (chapters 3 and 4), as retraction of a paper by itself has no nomenclatural consequence.[9–11] Using *O. khaungraae* as an example, there have been recommendations that the code needs to be modified to cover names and nomenclatural acts contained in retracted papers and to include a rule that can be applied automatically without the necessity of submitting a case.[12] Nonetheless, at the present time, the current regulations stand.

Diagnosis of the genus *Oculudentavis*

Oculudentavis can be identified as a lizard by having a pleurodont dentition with posterolingual tooth replacement, a short quadrate with a lateral conch, a streptostylic quadrate suspension, a "hockey stick"-shaped squamosal, a reduced quadrate-pterygoid contact, an enclosed vidian canal (posterior opening within the basisphenoid), a prootic with an alar process and a prominent crista prootica, and a braincase in which the metotic fissure is subdivided into a small ovoid lateral opening of the recessus scalae tympani and a posterior vagus foramen (differentiating it from archosaurs, where the metotic fissure becomes enclosed, following a totally different development).[13]

The genus *Oculudentavis* can be diagnosed by the following apomorphic characters. Some of these characters are reworded here from the original diagnosis of *O. khaungraae*[1] and some from a subsequent paper,[3] which now includes characters that

Please cite this article in press as: Bolet et al., Unusual morphology in the mid-Cretaceous lizard *Oculudentavis*, Current Biology (2021), https://doi.org/10.1016/j.cub.2021.05.040

CellPress
OPEN ACCESS

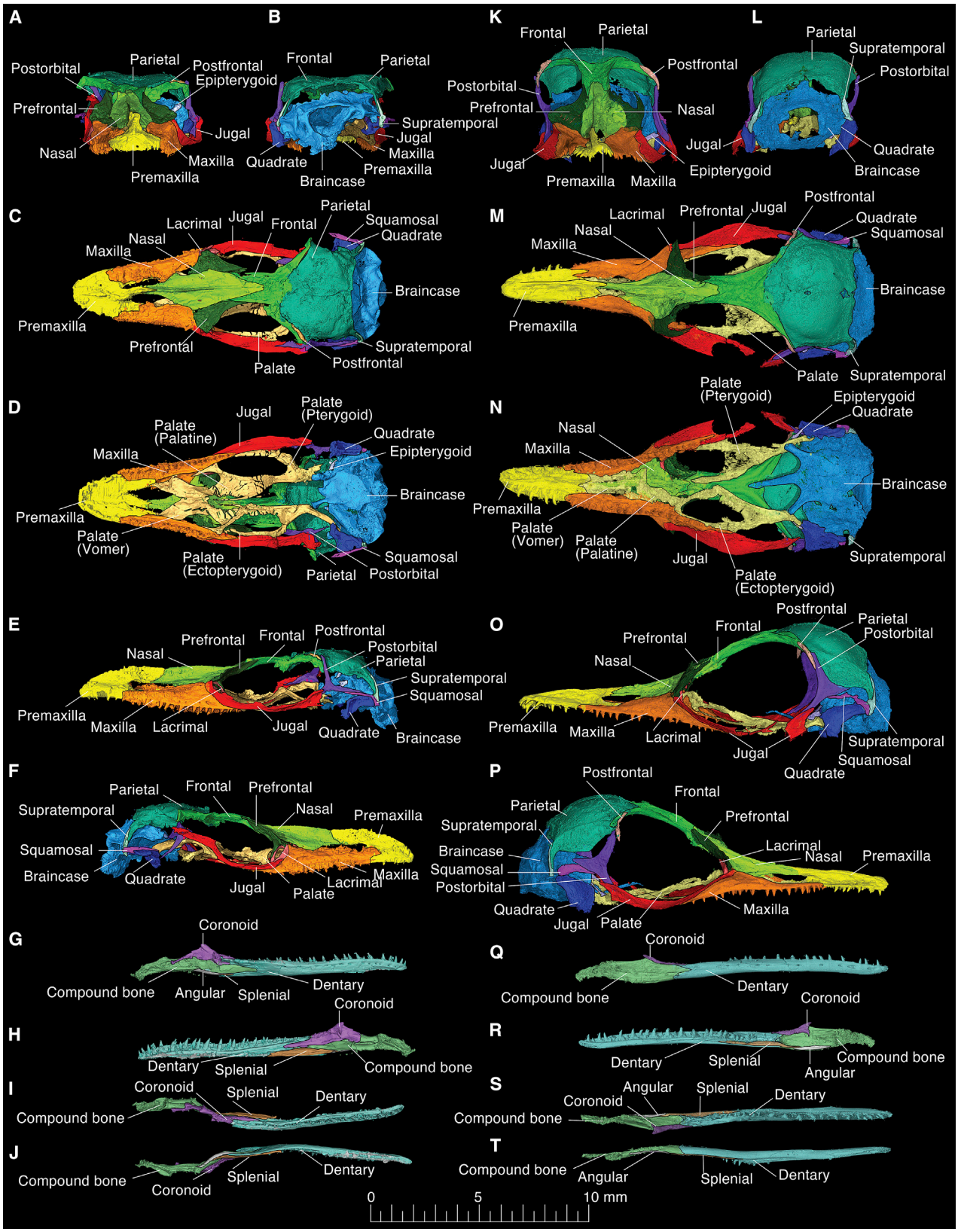

(legend on next page)

Please cite this article in press as: Bolet et al., Unusual morphology in the mid-Cretaceous lizard *Oculudentavis*, Current Biology (2021), https://doi.org/10.1016/j.cub.2021.05.040

only apply to *O. khaungraae*: jugal expanded horizontally creating a wide ventral orbital flange; jugal bar cross-section strongly angled dorsolaterally-ventromedially;[1] 22 to 23 teeth in maxilla, about four of which are located beneath the orbit; vomers contact both the premaxillary and maxillary shelves; large unpaired median premaxilla with a long dorsal crest along nasal process that is continued onto the dorsal surface of the nasals along most of its length; premaxilla replaces maxilla in anterolateral part of rostrum; ring-shaped lacrimal fully enclosing large lacrimal foramen; short vaulted parietals partially fused; and presence of a flat surface (forming a platform) on the dorsolabial side of the posterior third of the dentary.

Oculudentavis differs from all other known lizards in possessing the following unique combination of characters: premaxilla forming exclusively the tip of the rostrum and the anterolateral border of the nares; elongated paired nasals that slot into a triangular frontal recess; no parietal foramen, supratemporal processes angled vertically downward; strongly triradiate postorbital with long squamosal process reaching posterior margin of parietal; very large suborbital fenestra; palatal dentition on the pterygoids—differing from the interpretation in Li et al.,[3] which also reported teeth on the palatine, the presence of which we have been unable to confirm; in dentary, dorsal and ventral margins of the Meckelian fossa meet to close fossa, but do not fuse; and short postdentary region with coronoid bearing a low, posteriorly set process, short deep adductor fossa, and long slender retroarticular process.

Oculudentavis further differs from all squamates except *Huehuecuetzpalli* in having a long tapering rostrum[3] composed of premaxilla, maxillae, and elongated paired nasals that slot into a triangular frontal recess; from all squamates except for *Huehuecuetzpalli*, varanids, lanthanotids, monstersaurs, and mosasaurs in the retracted narial openings,[3] although in all but *Huehuecuetzpalli* a reduction of the nasals occurs; from all squamates except chameleons in having a prefrontal with an anterolateral shelf ("boss" in Gauthier et al.[7]) that overhangs maxilla and lacrimal; from all squamates except for the pygopodid *Lialis* in its very long slender mandible composed mainly of shallow elongate dentary and relatively short post-dentary portion; and from all squamates except for some anguimorphs in the presence of posterolingual tooth replacement. The closed (but not fused) Meckelian fossa is shared mainly with iguanians, differing from the open fossa of most anguimorphs, lacertoids, and scincoids and the closed and fused fossa of gekkotans, dibamids, gymnophthalmids, xantusiids, some scincids, and some iguanians.

The premaxilla, maxilla, and nasal are not fused into a single unit as was described in the original description of *O. khaungraae*.[1]

Oculudentavis khaungraae

Holotype

Hupoge Amber Museum, HPG-15-3, a complete skull preserved in amber (Figures 2K–2T, 3B, 3D, and S1). After its publication, we were given access to scan data of the holotype but do not have the authority to make it publicly available, although a rendering of this specimen can be accessed here: https://tinyurl.com/Oculudentavis-A-10420.

Type locality

Cenomanian 98.8 ± 0.6 Ma,[14] Aung Bar mine, Tanai Township (Myitkyina District, Hukawng Valley, Kachin province), northern Myanmar.

Diagnosis

Jugal process of maxilla that reaches caudally to at least the level of mid-orbit;[1] short squamosal process of the postorbital; large braincase with long, unexpanded basipterygoid processes on the basisphenoid; medial flange of pterygoid diverges posterolaterally along the entire length; interpterygoid vacuity heart shaped; premaxilla much longer than wide; recurved anterior marginal teeth (on premaxilla); and a well-developed flattened surface on the dorsolabial margin of the posterior portion of the dentary.

Oculudentavis naga new species

Holotype

Peretti Museum Foundation, GRS-Ref-28627, a skull and anterior postcranial skeleton (Figures 1, 2A–2J, 3A, 3C, and S1). Three-dimensional model of new specimen available at https://tinyurl.com/Oculudentavis-L-10420.

Type locality

The holotype specimen of *Oculudentavis naga* (GRS-Ref-28627) and the holotype of *O. khaungraae* (HPG-15-3) were recovered from the same mine (Aung Bar mine, 26° 09′ N, 96° 34′ E).

Etymology

Combination of *Oculudentavis* (oculus = eye, dentes = teeth, and avis = bird)[1] and Naga, the name of one of the many ethnic tribes living in the Burmese amber mines area. The Naga are mentioned in historical chronicles for their prominent role in amber trading. Divided into many sub-groups scattered across the hills and jungle of India (in Nagaland and other states) and in the Tiger valley region of Burma (where amber deposits are found), the Naga tribes are also reputed for their rich and fascinating culture.

Diagnosis

The holotype of *O. naga* (skull length = 14.2 mm) is somewhat smaller than that of *O. khaungraae* (skull length = 17.3 mm). *Oculudentavis naga* differs from *O. khaungraae* in having a jugal process of the maxilla that reaches caudally to less than 25% of orbit length; in having a long squamosal process of the postorbital; in having a relatively smaller braincase, with short, distally expanded basipterygoid processes (versus longer, unexpanded processes); and in having anterior palatal rami of pterygoids parallel, diverging posteriorly just behind the fossa columellae, interpterygoid vacuity nearly rectangular (versus divergent pterygoids, heart-shaped vacuity), rostral part of premaxilla shorter and proportionally wider than that of *O. khaungraae*, and less conspicuous platform on the dorsolabial surface of the posterior third of the dentary.

Notes

There are also differences between the two specimens in the robusticity of the postorbital (greater in *O. khaungraae*); the height

Figure 2. Comparison of the two specimens of *Oculudentavis*, each bone digitally segmented

Synchrotron HRCT of *O. naga* (A–J) and *O. khaungraae* (K–T). (A and K) Anterior view, (B and L) posterior view, (C, M, I, and S) dorsal view, (D, N, J, and T) ventral view, (E and O) left lateral view, (F, G, P, and Q) right lateral view, and (H and R) medial view are shown. See also Figures S1–S7 and Data S1.

Please cite this article in press as: Bolet et al., Unusual morphology in the mid-Cretaceous lizard *Oculudentavis*, Current Biology (2021), https://doi.org/10.1016/j.cub.2021.05.040

CellPress
OPEN ACCESS

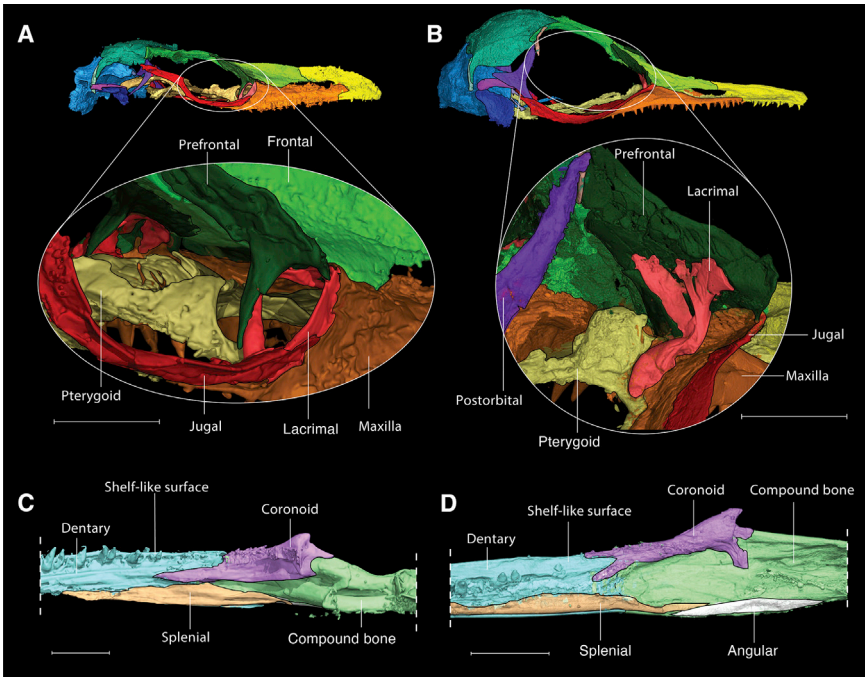

Figure 3. Comparison of the two specimens of *Oculudentavis*, details of the lacrimal and dentary

Right side view of the orbit showing the ring-like lacrimal bone (salmon color) *in situ* in (A) *O. naga* and (B) *O. khaungraae* (orbit view here is posterolateral to show the orbital elements more clearly). Dorsolingual view of the dentary in (C) *O. naga* and (D) *O. khaungraae* is shown. Scale bar represents 1 mm.

of the premaxillary crest (greater in *O. naga*); the extent of the nasal emargination of the frontal (greater in *O. naga*); the presence of a large anterior palatine fenestra (*O. naga*); the length and height of the coronoid process (larger and taller in *O. naga*); the shape of the quadrate conch (more angular in *O. khaungraae*); and in the overall shape of the rostrum (more pointed in *O. khaungraae*) and postorbital skull (more vaulted in *O. khaungraae*). *Oculudentavis naga* also displays a very large palatal fenestra between the vomers and palatines. This region is poorly preserved in the holotype of *O. khaungraae*, and the presence or absence of the fenestra cannot be determined. However, it is possible that at least some of these differences between the two specimens are due to a combination of individual variation, taphonomical deformation (also rendering some elements difficult to segment precisely), and perhaps sexual dimorphism (comparing a male of one species with a female of another could exaggerate interspecific differences like the premaxillary crest height). With only a single specimen of each species, individual variation is impossible to assess. Also note that the skull of *O. khaungraae* was reported as measuring 14 mm in length,[1] whereas our own measurement of the specimen gives a length of 17.3 mm.

Description

In its bird-like shape (vaulted cranium and tapering rostrum), the skull of *Oculudentavis khaungraae* appears strikingly different from that of any known lizard (Figure 4). The bird-like appearance is less striking in *O. naga*, which has a less compressed rostrum (Figure 2).

Despite the compression of the rostrum, the two species share many characters that distinguish them from other lizards. The nares are bounded by the premaxilla anterodorsally, the maxilla posteroventrally, and by the nasals posteriorly. The location of the nares is also the same, being placed at mid-length of the antorbital region and in having an elongated oval shape. The orbit is more intact in *O. khaungraae*, being nearly circular. In both species, the longest axis of the orbit is about 1/3 the total length of the skull and the orbit is complete and separated from the temporal fenestrae by a complete postorbital bar. The parietal supratemporal processes are aligned with the long and slender vertical supratemporals and fail to meet the squamosals ventrally. There is a complete circumorbital series in both specimens—jugal (ventrally), lacrimal (anteriorly), prefrontal (anterodorsally), frontal (dorsal), postfrontal (posterodorsally), and postorbital (posteriorly).

Premaxilla (Figures 2, S2A–S2B, S2I, and S2J). The upper jaw comprises an unpaired median premaxilla with slender, pointed teeth (9 in *O. khaungraae* and ~10 in *O. naga*; count refers to one side of the element). The more anterior premaxillary teeth appear recurved in *O. khaungraae*, but the equivalent teeth in *O. naga* are partially obscured. Both species have a long crest along the premaxillary nasal process (the crest was considered taphonomic in *O. khaungraae*),[1] which continues onto the nasals. The palatal shelf is broad and flat and has two narrow palatal processes that bound a large premaxilla-vomer fenestra in *O. naga*, which has a less deformed palate. The palatal processes of the premaxilla are also visible in *O. khaungraae*, but not the intervening fenestra (see below).

Maxilla (Figures 2, S2C–S2E, and S2K–S2M). The maxilla of both species has a low, medially curved facial process, a long rostral component, and a suborbital ramus that does not reach the posterior margin of the orbit—extending up to one-quarter of the orbit length in *O. naga* and to about mid-orbit in *O. khaungraae*. It is excluded from the orbital rim by the jugal. The maxillary teeth are conical and pointed. There are 24 to 25 tooth maxillary loci in *O. naga* and 27–29 in *O. khaungraae*. The maxilla has two horizontal facets: one to support the prefrontal and another for the jugal.

Nasal (Figures 2, S2F, and S2N). The paired nasals form a rhomboid plate, and combined with the maxilla, they define a long tapering rostrum with retracted narial openings. The nasals are paired, but they exhibit partial fusion along the crest and remain separated posterior to the crest.

Prefrontal (Figure 2). The prefrontals comprise a flat anterodorsal plate and a weakly concave orbital plate, contacting the ring-shaped lacrimal ventrally. The anterodorsal plate seems less

Please cite this article in press as: Bolet et al., Unusual morphology in the mid-Cretaceous lizard *Oculudentavis*, Current Biology (2021), https://doi.org/10.1016/j.cub.2021.05.040

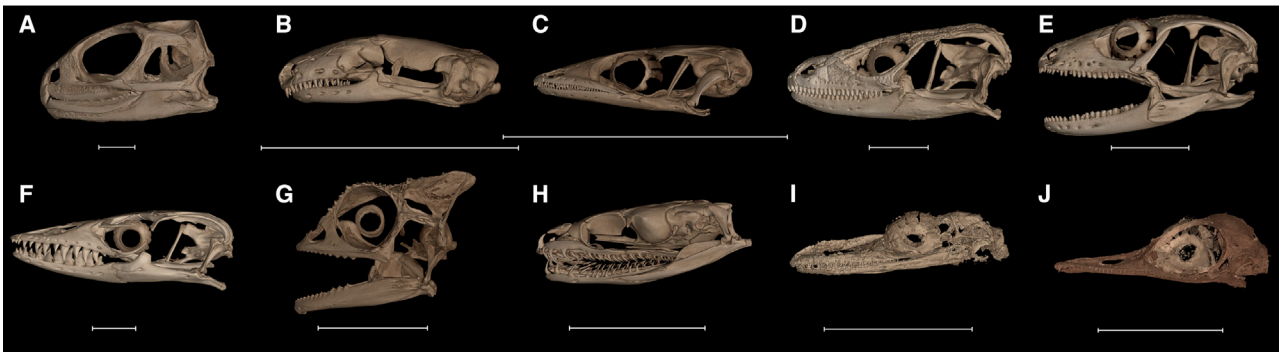

Figure 4. Cranial disparity of typical lepidosaurs to demonstrate the atypical skulls of *Oculudentavis*

(A) *Sphenodon punctatus*, Rhynchocephalia UF11978; (B) *Anelytropsis papillosus* UF-H-86708, Dibamidae; (C) *Sphaerodactylus caicosensis* UF95971, Gekkota; (D) *Smaug swazicus* NMB-R9201, Cordyliformes; (E) *Eugongylus albofasciolatus* CAS159825, Scincidae; (F) *Varanus* sp. UF71411, Varanidae; (G) *Rieppeleon brevicaudatus* CAS168891, Iguania; (H) *Boaedon fuliginosus* CAS85747, Serpentes; (I) *Oculudentavis naga* GRS-Ref-28627; (J) *O. khaungraae* HPG-15-3. Scale bar represents 10 mm.

developed in *O. khaungraae* than *O. naga*. The lateral edge of the anterodorsal plate projects as a short angular (*O. naga*) or ridge-like (*O. khaungraae*) shelf that overhangs the lacrimal and maxilla. This shelf is autapomorphic among lizards, with a ridge, crest, or boss in this position variably present (e.g., some iguanians, including chameleons; some *Phrynosoma*; and some *Anolis*).

Lacrimal (Figures 3A and 3B). The lacrimal of both species is unique among lizards and is one of several distinctive features that demonstrates their close relationship. It forms a ring, completely enclosing a large lacrimal foramen.

Jugal (Figures 2, S2G, S2H, S2O, and S2P). In both species, the jugal forms a dorsomedially expanded flange that provides ventral support to the large eye. The orientation of the jugal is unusual for squamates, being dorsomedially inclined. The postorbital process of the jugal is short (distorted on the right side of *O. naga*).

Frontal (Figures 2, S3A, and S3E). In both species, the unpaired median frontal has weak sub-olfactory processes and a deep V-shaped anterior emargination that receives the nasals. The frontal is overlapped extensively by the nasals, reaching the level of the mid-orbit in *O. naga* and somewhat less in *O. khaungraae*. The supraorbital margins are subparallel and diverge posterolaterally, establishing a broad contact with the anterior margin of the parietal. The structure of the posteromedial margin of the fronto-parietal suture is unclear in both specimens (Figure 2, dashed lines).

Parietal (Figures 2, S3B, and S3F). The parietals are short and partially fused (separated posteriorly). They have a rounded lateral profile, lack a parietal foramen, and have short supratemporal processes that curve ventrally rather than posteriorly to meet the supratemporals. This portion of the skull contacts the short paroccipital processes of the otoccipital. Li et al.[3] argued that the small opening in the midline of the parietals in the holotype of *O. khaungraae* corresponds to a parietal foramen, but it is irregular and appears to be an artifact of breakage.

Postfrontal (Figure 2). The postfrontal is a small, splint-like bone, lateral to the frontal and the parietal in *O. khaungraae* but of uncertain structure and position in *O. naga*. The postfrontals are very reduced in both species and were not noticed in the original description of *O. khaungraae*.

Postorbital (Figures 2, S3C, and S3G). The postorbital is a strongly triradiate bone with a long (*O. naga*) or short (*O. khaungraae*) posterior process that contacts the squamosal posteriorly. The postorbital differs in the two species: the postorbital squamosal process tapers gradually in the *O. naga* holotype, while the tapering appears more abrupt in the *O. khaungraae* specimen. Due to the proportionally thicker postorbital, the right side of *O. khaungraae* shows a more extensive contact between the postorbital and the descending process of the parietal, entirely covering the braincase laterally and almost completely closing the upper temporal fenestra. However, on the left side, it is clear that this fenestra remained open. In *O. naga*, the upper temporal fenestra looks larger, but the skull table of this specimen is very depressed and the postorbital is more gracile, so the differences in configuration of the upper temporal bar may be exaggerated by taphonomic deformation.

Squamosal (Figures 2, S3D, and S3H). In both species, the typically squamate hockey-stick-shaped squamosal lacks an ascending process and lies between the supratemporal, the postorbital, and the quadrate.

Supratemporal (Figures 2, S3B, and S3F, articulated with the parietal). The supratemporal is also reduced to a slender vertical splint of bone that contacts the lateral margin of the parietal supratemporal process, separating it from the squamosal.

Palate (Figures 2, S4A, and S4D). In the palate of *O. khaungraae*, the premaxilla-vomer fenestra is totally obliterated (due to compression). In this respect, *O. naga* has a more intact rostrum, more clearly exhibiting the premaxilla-vomer fenestra and the very large fenestra exochoanalis. The suborbital fenestra is oval in both specimens and is bounded by the same bones: palatines anteromedially, ectopterygoids laterally, and pterygoids posteriorly, although the sutures between these bones are not easy to identify. It also looks as if the ectopterygoid barely contacts the palatine in *O. naga*, but the degree of contact is ambiguous in *O. khaungraae*. The shape of the interpterygoid vacuity differs between the two species. Pterygoid teeth are present and are arranged in a row on the anteromedial process of the pterygoid, just posterior to the inferred suture with the palatine. There are about 3 to 4 on each bone in *O. khaungraae*; the

Please cite this article in press as: Bolet et al., Unusual morphology in the mid-Cretaceous lizard *Oculudentavis*, Current Biology (2021), https://doi.org/10.1016/j.cub.2021.05.040

same area is fragmented in *O. naga*, but small projections on both pterygoids can be interpreted as pterygoid teeth.

Quadrate (Figures 2, S4B, and S4E). The quadrate is distinctively low in position and small in size in both species. The quadrate is stouter in *O. khaungraae* (with a more prominent head) than in *O. naga*, but the overall shape is similar in both specimens, with a shallow conch, a slightly curved medial pillar, and a lateral tympanic crest that has a 90-degree angulation along its length. The quadrate suspension in both species is characteristically squamate.

Braincase (Figures 2 and S5). By comparison with that of *O. khaungraae*, the braincase of *O. naga* is unevenly dorsoventrally compressed, so that the right side is more damaged than the left and the posteroventral margin is abnormally low. Nonetheless, comparison of the two braincases shows more similarities than differences, notably the well-developed crista prootica, short alar processes, slender basipterygoid processes, short basisphenoid, enclosed vidian canals opening posteriorly within the basisphenoid, robust parasphenoid rostrum (base only preserved in *O. naga*), short uncrested supraoccipital with a visible processus ascendens (mineralization uncertain), and short paroccipital processes. The parasphenoid rostrum is well preserved in *O. khaungraae*, being longer than the basipterygoid processes, and almost entirely divides the interpterygoid vacuity. In *O. naga*, the parasphenoid rostrum is represented only by its base, possibly due a fracture or weak mineralization. However, there are differences in the orientation, length, and distal shape of the basipterygoid processes in the two species.

Epipterygoid (Figure 2). These elements are poorly preserved and displaced in both species. They are columnar and still in articulation within the fossa columellae of the pterygoid, this articulation being another uniquely squamate character. In the holotype of *O. naga*, a portion of the left epipterygoid remains attached to the alar process.

Scleral ossicles (Figures 1, S4C, and S4F). In both species, the orbit contains a large ring of "spoon-shaped" scleral ossicles that supported a large eye. The ossicle count is 14 in both specimens. Due to the distinctive shape of the ossicles, they overlap at both their inner edges (which would have surrounded the iris and the pupil) and the outer edges, leaving oval gaps between ossicles in the middle of the sclerotic ring. Although the skull of *O. khaungraae* is 1.2× longer than that of *O. naga*, the scleral ossicles are proportionally larger in *O. khaungraae,* being 1.5× larger than those of *O. naga*.

Dentary (Figures 2, 3C, 3D, and S6). Both species have a long shallow mandible of which the straight dentary forms the major part (~75%) and a large number of sharp, weakly pleurodont teeth (29 to 30 in both specimens). Both species also have a large number of lateral neurovascular foramina (10–12), and the dentary in each specimen has parallel upper and lower margins. The symphyseal region does not extend beyond the second tooth locus in either specimen. The lower margin of the dentary curves dorsomedially and closely approaches the subdental shelf, thus restricting the Meckelian fossa but without fusion. The Meckelian fossa remains open posteriorly, where it is overlapped by the splenial. The dorsolabial surface of the posterior one-third of the dentary bears a flattened, shelf-like surface.

Splenial (Figures 2 and S6). The splenial is very slender and does not extend anteriorly beyond the posterior one-third of the dentary, closing only the posterior part of the Meckelian fossa in both species. Posteriorly, the splenial does not extend beyond the level of the coronoid eminence.

Coronoid (Figures 2 and S6). The postdentary region is short, including a coronoid with a low, posteriorly set, coronoid eminence. The coronoid looks significantly larger in the holotype of O. *naga* than in the holotype of *O. khaungraae*, especially in the development of the anterolateral and anteromedial processes. However, these differences could be due to damage during deformation, making it difficult to establish clear bone boundaries (e.g., between surangular and coronoid), as this was one of the most problematic regions to segment in both specimens.

Angular (Figures 2 and S6). This is a very reduced and slender bone, limited to the posteroventral side of the jaw.

Compound bone (Figures 2 and S6). There is no obvious suture between the surangular and the articular or prearticular in either specimen. Both specimens have a long retroarticular process and a short, deep adductor fossa. It is uncertain whether the coronoid reached the anterior margin of the adductor fossa.

Although only part of the postcranial skeleton is preserved in *O. naga*, it shows a short neck with eight cervical vertebrae that are amphicoelous, atlantal arches bearing posterior zygapophyses, and a pectoral region comprising a T-shaped interclavicle, medially expanded clavicles, and a typically squamate scapulocoracoid with scapular, scapulocoracoid, and primary coracoid fenestrae.

Vertebrae (Figures S7A and S7B). Eight cervical vertebrae are preserved, including the atlas and the axis, as well as a small number of dorsal vertebrae (using the traditional anatomical definition whereby the first dorsal vertebra is that with a rib that meets the sternum, contra Gauthier et al.[7]). The atlantal arches are not fused, and they have well-developed postzygapophyses. The axis preserves the dens, which is already fused in place. The vertebrae are amphicoelous and notochordal, with low neural spines. There are simple semicircular intercentra visible in the anterior part of the neck, with only a weak ventromedian keel (Figure S7). As in living gekkotans, these elements are free and intercentral in position. The first visible cervical rib is on cervical six, but there may have been ribs more anteriorly. There are no gastralia.

Clavicle (Figure S7C–S7E). The clavicles are expanded medially and have a well-defined clavicular fenestra completely enclosed by bone. The clavicles are separated at the ventral midline by tip of the T-shaped interclavicle. Dorsally, the clavicles appear to extend above the level of the scapula blade, possibly meeting a suprascapular cartilage.

Scapulocoracoid (Figures S7C–S7E). Both scapulocoracoids are preserved and display an anterior primary coracoid emargination, an emarginated scapular blade, and a large circular scapulocoracoid emargination. Dorsal to the scapula, there is an irregular mass that may represent the suprascapular cartilage.

Sternum (Figure S7D). Only the anterior border of the cartilage sternum is preserved, suggesting it was rhomboid.

Interclavicle (Figure S7D). The interclavicle is T-shaped and quite robust.

Humerus (Figure S7D). The proximal portion of the left humerus is present, preserving the humeral head and the lateral tuberosity.

Please cite this article in press as: Bolet et al., Unusual morphology in the mid-Cretaceous lizard *Oculudentavis*, Current Biology (2021), https://doi.org/10.1016/j.cub.2021.05.040

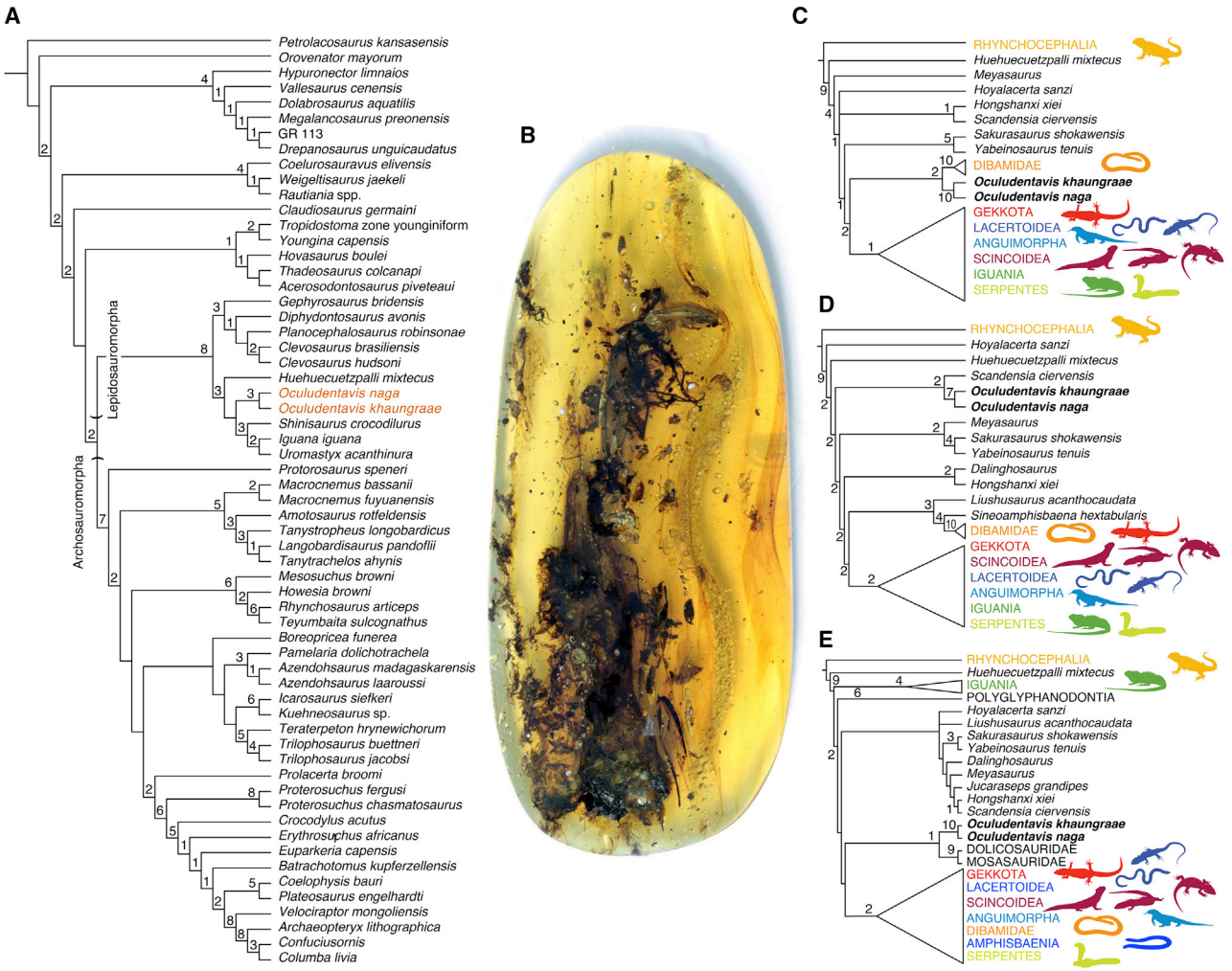

Figure 5. Phylogenetic trees showing the position of *Oculudentavis*

(A) Phylogenetic tree showing the position of *Oculudentavis* using an amniote dataset;[6] (B) photograph of the holotype of *O. naga*; (C) simplified phylogenetic tree showing the position of *Oculudentavis* using a squamate dataset[7] combined with a molecular dataset[15] treating some morphological characters as ordered; (D) simplified phylogenetic tree showing the position of *Oculudentavis* using the same dataset as in (C) but with all characters unordered; (E) simplified phylogenetic tree showing the position of *Oculudentavis* using the same dataset as (C) but removing molecular data. In (C)–(E), crown groups were collapsed and are represented by silhouettes. *Sphenodon punctatus*, *Anelytropsis papillosus* (Dibamidae), *Sphaerodactylus klauberi* (Gekkota), *Smaug giganteus* (Cordylidae), *Xantusia vigilis* (Xantusiidae), *Tribolonotus gracilis* (Scincidae), *Bachia flavescens* (Lacertoidea), *Lacerta bilineata* (Lacertoidea), *Blanus cinereous* (Amphisbaenia), *Varanus komodoensis* (Anguimorpha), *Physignathus cocincinus* (Iguania), and *Ophiophagus hannah* (Serpentes) are shown. Node values indicate Bremer support; nodes with no support were recovered in the implied weights analyses. See also Data S1.

Soft tissue (Figure 1; Data S1, Gular scales in *Oculudentavis*). Both specimens also preserve soft tissue. The head and body are covered in small, granular scales, with large rectangular supralabial and infralabial scales, tiny scales covering the eyelid, and a nostril placed anterior to the midpoint of each retracted narial opening (Figures 1 and 2) in *O. naga*. There are no osteoderms. On the ventral surface of the head in *O. naga*, along the midline, the epidermal scales are raised and form a line of evenly spaced short ridges. Posterior to this midventral line, the skin of the gular region is thrown into a series of narrow linear folds. This folded region underlies the hyoid ceratobranchials and may demonstrate the resting anatomy of loose gular skin that could be inflated, for example in territorial display, in association with hyoid movements.

Phylogenetic and morphospace position

To test the interpretation of squamate status for *Oculudentavis*, we scored both specimens into two datasets: (1) an amniote dataset that includes archosauromorphs and lepidosauromorphs[6] with the addition of a non-avian theropod, a crocodylomorph, two stem-birds, and a crown-bird (Figure 5A) and (2) a large morphological data matrix focused on Squamata[7] with the inclusion of molecular data (Figures 5C and 5D; Data S1, Combined evidence tree for squamate dataset using the ordered scheme and Combined evidence tree for squamate dataset using the unordered scheme).[15] In the phylogenetic analysis of the amniote dataset, GRS-Ref-28627 and HPG-15-3 consistently and unequivocally group as sister taxa, a position compatible with attribution of

Please cite this article in press as: Bolet et al., Unusual morphology in the mid-Cretaceous lizard *Oculudentavis*, Current Biology (2021), https://doi.org/10.1016/j.cub.2021.05.040

CellPress
OPEN ACCESS

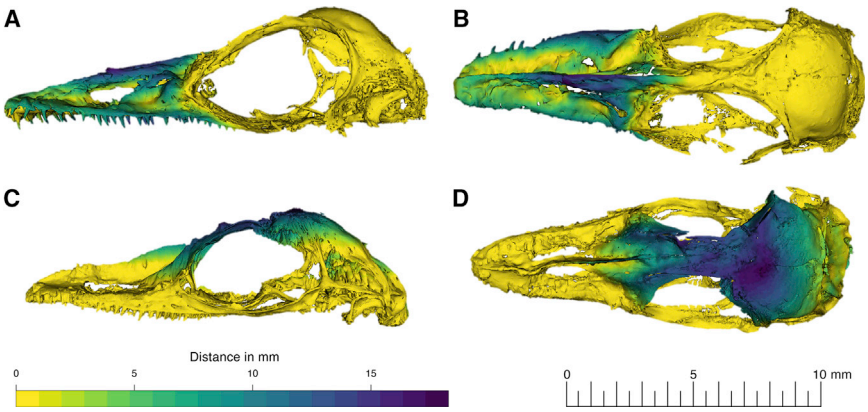

Figure 6. Heatmaps displaying the possible degree of deformation in *Oculudentavis* species

O. khaungraae HPG-15-3 (A and B) and *O. naga* GRS-Ref-28627 (C and D). The shape variation (degree of deformation) between the original and retrodeformed 3D surface is color coded, with yellow and dark blue representing no deformation and high deformation, respectively. Heatmaps indicating the amount of retrodeformation provide a good visual aid to display the regions where a specimen would have been deformed and what its overall shape would have looked like prior to deformation. All changes are based on observed distortions in the specimens themselves. See also Data S1.

GRS-Ref-28627 to *Oculudentavis*, and this genus always clusters with squamates (Figure 5A). Both specimens show an unequivocal suite of unique squamate characters. A phylogenetic analysis constraining *Oculudentavis* as a bird, but without any defined location, resulted in *Oculudentavis* being placed basal to a clade formed by *Archaeopteryx*+*Confusiusiornis*+*Columba*. This analysis found four trees that were 28 steps longer than the 9 trees of the unconstrained analysis (1,164 steps [constrained] versus 1,136 steps [unconstrained]). The same constrained and unconstrained analyses were run using implied weights (k = 20). In these analyses, the tree distortion in the constrained analysis increased from 33.58 to 34.92. Both implied weights analyses recovered only one tree. If the difference in fit is scaled with the best score, the difference is 0.0246 in the case of equal weights, whereas for implied weights, it is 0.0349.

As it stands in the present phylomorphospace plot, a subtle convergence is apparent between birds, squamates, and drepanosaurs (Data S1, 2D phylomorphospace using the amniotes matrix), rather than between *Oculudentavis* and birds. Morphological convergence between *Oculudentavis* and birds was more obvious in our initial results (not shown) but gradually became diffuse as more information was added from improved segmented models. Adding the third axis (PCO3) does not show a clearer convergence between birds and squamates or *Oculudentavis* (Data S1, 3D phylomorphospace using the amniote matrix). An analysis corresponding to the skull characters alone, which was expected to concentrate the convergent features between *Oculudentavis* and birds, also failed to show any convergence. Orienting the 3D plot of the skull dataset to see PCO1 against PCO3 (Data S1, 3D phylomorphospace using the amniote matrix) again shows some convergence between birds and squamates as a whole, but not *Oculudentavis* in particular.

The phylogenetic analysis of Gauthier et al.'s squamate matrix (combined with molecular data) with additive characters recovers *Oculudentavis* as sister to dibamids (Figure 5C). *Jucaraseps* is the only identified wildcard taxon, causing a polytomy for non-dibamid squamates. An analysis of the same matrix using unordered characters recovers *Oculudentavis* as forming part of the stem of Squamata, specifically as sister to *Scandensia* (Figure 5D). Finally, removing the molecular data (and thus using morphology alone) places *Oculudentavis* as sister to mosasaurs (Figure 5E), which are on the stem of "Scleroglossa" (non-iguanian squamates).

Distortion of the specimens

Xing et al.[1] considered their specimen of *Oculudentavis khaungraae* to be skeletally mature, and this is probably true of the *O. naga* holotype, given the tight connections between bones, the closed parietal and basicranial fontanelles, the conjoined scapula and coracoid, the sutured humeral epiphysis, and the fused dens of the axis. *O. khaungraae* has a relatively larger eye than *O. naga* and appears to have a much shallower rostrum and a more vaulted parietal, but the latter two differences may be artifacts of preservation. Both specimens have undergone compression but in different ways and in different parts of the skull. The specimen of *O. khaungraae* has suffered compression of the rostrum. The "dented" prefrontals and the out-turned maxillary teeth on the right side provide clear evidence of this, as does the fact that the teeth of the left dentary have pushed through the maxilla of that side. In an anterior view of the *O. khaungraae* skull,[1] the jaw outlines are seen to be distorted, and the twisting of the dentary is seen clearly in the disarticulated right mandible. In contrast, *O. naga* has experienced compression of the orbital region and posterior skull, as shown by the upward displacement of the dorsal tip of the left postorbital, the broken jugal, and the disparity in height between the dorsal edge of the scleral ring and the frontal (suggesting the eyeballs may have been pushed outward when the head was compressed). Together, these points of damage exaggerate the differences in height between the rostrum, orbit, and postorbital skull in the two specimens. Thus, the proportional differences between the skulls could be due to a combination of interspecific differences (e.g., premaxillary length) as well as differences in size, taphonomy, and even sexual dimorphism.[16] Although sexual dimorphism primarily relates to discussion of intraspecific variation, it is also relevant to interspecific comparison. Given two closely related sexually dimorphic species (e.g., within the extant *Basiliscus* or *Trioceros*), comparison between a male of one and a female of the other would exaggerate the interspecific differences. *Oculudentavis naga* has a taller premaxillary crest, giving the rostrum a deeper (and less bird-like) appearance. The more pronounced premaxillary crest could, potentially, be a sexually dimorphic trait (e.g., if the *O. naga* specimen is male), if not meaningful at interspecific level. Based on the observed deformations of the skulls described above and obvious asymmetries between left and right sides, we used new retrodeformation methods on landmark data of the two specimens to provide a proof of concept that some of

Please cite this article in press as: Bolet et al., Unusual morphology in the mid-Cretaceous lizard *Oculudentavis*, Current Biology (2021), https://doi.org/10.1016/j.cub.2021.05.040

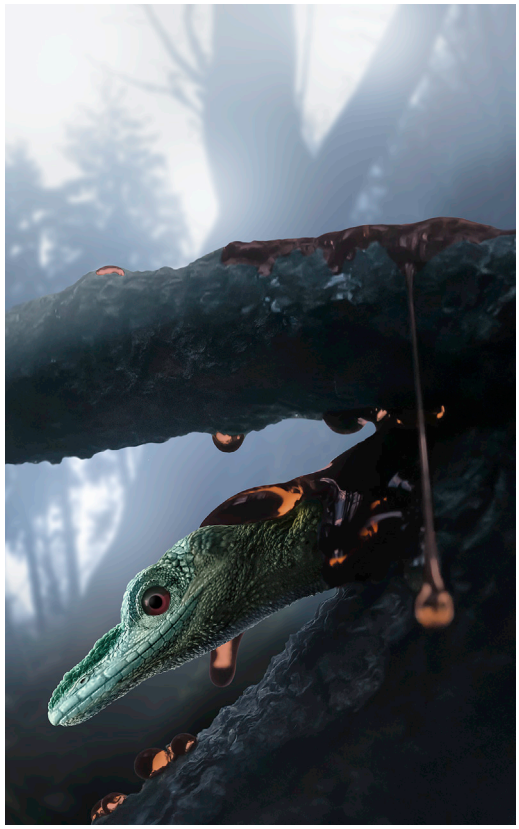

Figure 7. *Oculudentavis naga* prior to being trapped in tree resin
Scientific illustration by Stephanie Abramowicz.

the differences between the skulls of *O. khaungraae* and *O. naga*, including the more bird-like appearance of the former, could, at least in part, be an artifact of lateral compression of the rostrum. The heatmap plots on the retrodeformed meshes support the proposal that some of the overall proportional differences between the *O. khaungraae* and the *O. naga* holotypes can be explained by taphonomic deformation (Figure 6). The *O. khaungraae* heatmap displays greater deformation of the rostrum (Figures 6A and 6B), whereas the *O. naga* heatmap shows that most of the deformation was concentrated on the vault of the skull (Figures 6C and 6D).

Retrodeformation methods permit the marked differences between specimens (based on observable distortions and asymmetries) to be corrected, resulting in more similar skull proportions. This is congruent with the highly distinctive features shared by these two specimens and supports the generic allocation. Moreover, the bird-like appearance of *O. khaungraae* becomes less striking once this deformation is corrected. However, considering the osteological differences in the palate and postorbital bones, we have opted to place these two specimens into separate species. This may be re-assessed if further specimens are recovered.

DISCUSSION

The morphological features described above and the phylogenetic analyses support the identification of GRS-Ref-28627 as a second species of the genus *Oculudentavis*, which is an unusual squamate rather than a bird. Using a squamate dataset combining both morphological and molecular data, the phylogenetic placement of both species of *Oculudentavis* within Squamata is markedly different, depending on how the data are treated. If the characters are treated as ordered, the two specimens form a sister clade to the limb-reduced, vestigial-eyed, fossorial Dibamidae, near the base of Squamata (Figure 5C; Data S1, Combined evidence tree for squamate dataset using the ordered scheme). If characters are treated as unordered, then *Oculudentavis* is recovered on a rather populated stem of Squamata (Figure 5D; Data S1, Combined evidence tree for squamate dataset using the unordered scheme), which mainly comprises early-middle Cretaceous taxa. This position fits the results recovered in the analysis of the amniote dataset phylogenetic analysis, where *Oculudentavis* is on the stem of Squamata, one node above the Cretaceous *Huehuecuetzpalli*. When molecular data are removed, *Oculudentavis* is recovered as sister to mosasaurs, on the stem of "Scleroglossa." Unfortunately, the ancestral skull morphology of mosasaurs is poorly known. There is currently no confirmed pre-Cretaceous record for mosasaurians, and most early-mid Cretaceous mosasaurian taxa have poorly preserved, or absent, skulls. *Oculudentavis* shares a long ascending nasal process of the premaxilla and retraction of the narial openings with mosasaurs but differs from them in most other respects, including (in *Oculudentavis*) the shape of the quadrate, the short parietal, absence of a parietal foramen, ventrally oriented supratemporal processes, broad vomers, long dentary, amphicoelous vertebrae, and fenestrated scapula.[17,18]

It is notable that many of the characters that diagnose *Oculudentavis* are not unusual among stem birds and/or their modern descendants: large median premaxilla; long tapering rostrum composed of premaxilla, maxillae, and elongated paired nasals; retracted narial openings; co-ossified vaulted parietals and median frontal; no parietal foramen; large orbit containing prominent scleral ossicles; short paroccipital processes; and short postdentary region with coronoid bearing a low, posteriorly set process and long slender retroarticular process. However, convergence between lizards (as a whole) and birds is only weakly illustrated in the phylomorphospace analysis (Data S1, 2D phylomorphospace using the amniotes matrix). Given the obvious differences in postcranial morphology between birds and lizards, we repeated the phylomorphospace analysis using only skull characters. However, limiting the morphospace to the cranial material did not reveal a clearer pattern of convergence (Data S1, 3D phylomorphospace using the amniote matrix). Although a degree of convergence can be observed in the plot of PCO1 against PCO3 (as shown in the 3D phylomorphospace of the cranial dataset; Data S1, 3D phylomorphospace using the amniote matrix), it concerns birds and squamates as a whole, not *Oculudentavis* in particular. These results suggest that the similarity between the holotype of *Oculudentavis khaungraae* and the skull of birds has more to do with the proportions of the skull (e.g., the large orbits, vaulted skull roof, or elongate rostrum) as exaggerated by deformation than with the presence of shared derived character states, at least regarding the amniote matrix used.

The absence of substantial postcranial material for *Oculudentavis* limits our ability to reconstruct its lifestyle. The large eyes

with small pupils (Figures S4C and S4F) suggest *Oculudentavis* was diurnal, dwelling in photopic light environments,[1,19,20] and, given its entrapment in amber, may have been arboreal (Figure 7), but this remains speculative. The mechanical advantage of a lizard jaw depends on the ratio between the distance of the jaw joint to the point of application of the adductor muscles (in-lever) and the length of the jaw as a whole (out-lever).[21] Jaws in which the tooth row is of similar length to the distance between the coronoid process and the jaw articulation will deliver a stronger bite than one in which the tooth row is several times longer than the post-coronoid jaw, as it is in *Oculudentavis*. The long shallow dentary, sharp conical teeth, low coronoid process, weak mandibular symphysis, restriction of adductor muscle origin to lateral parietal margins, and the short mandibular adductor fossa are suggestive of a weak bite force. Coupled with the long retroarticular process, for the attachment of the depressor mandibulae, this implies a feeding strategy requiring fast jaw opening but limited power—perhaps for snapping at fast-moving small insects (e.g., ants or flies; Figure 1). This would be consistent with the large eyes and tapering rostrum.

Our retrodeformation results (Figure 6) provide a proof of concept that the bird-like appearance of the HPG-15-3 skull is plausibly an artifact of lateral compression of the rostrum. Furthermore, they also demonstrate that virtual retrodeformation methods can provide a complementary procedure to aid traditional osteological analyses in fossil descriptions. Therefore, herein (STAR Methods), we present a streamlined workflow for virtual retrodeformation of taphonomically deformed specimens, based on 3D landmark data.

With new lizard specimens emerging from the Myanmar amber each year, new specimens of *Oculudentavis* may yield additional material of the postcranial skeleton, notably the pelvic region, distal parts of the limbs, and tail, providing further ecomorphological data on this unusual lizard and further resolution of its phylogenetic position.

STAR★METHODS

Detailed methods are provided in the online version of this paper and include the following:

- KEY RESOURCES TABLE
- RESOURCE AVAILABILITY
  - Lead contact
  - Materials availability
  - Data and code availability
- EXPERIMENTAL MODEL AND SUBJECT DETAILS
  - Ethics statement
- METHOD DETAILS
  - Spectroscopy and stratigraphic data
  - Synchrotron Scanning
  - Phylogenetic analysis
  - Phylomorphospace analysis
  - Retrodeformation analysis

SUPPLEMENTAL INFORMATION

Supplemental information can be found online at https://doi.org/10.1016/j.cub.2021.05.040.

ACKNOWLEDGMENTS

We are grateful to the Peretti Museum Foundation for access to their collection of fossils in amber from Myanmar. We thank Jessica A. Maisano and Matthew Colbert from the UTCT—University of Texas—High-Resolution X-Ray CT Facility for the scanning of the referred specimen. We also thank Lida Xing and Jingmai O'Connor for sharing the data of the holotype of *O. khaungraae*, to Gang Li at the Beijing Synchrotron Radiation Facility for facilitating the transfer of the large dataset, and to the Australian Nuclear Science and Technology Organisation, where synchrotron images of the referred specimen were acquired. We also thank Dr. Krister T. Smith (Senckenberg Research Institute), Dr. Michael Caldwell (University of Alberta), and two anonymous reviewers for their comments that helped improve the quality of this manuscript. J.D.D. was funded by the National Science Foundation (DEB 1657656) and the Biological Sciences Department at Sam Houston State University; A.B. was funded by a Newton International Fellowship (NF170464, funded by the Royal Society), a Juan de la Cierva Incorporación Fellowship (IJC2018-037685-I, funded by Ministerio de Ciencia e Innovación of the Spanish Government), and the CERCA programme; and A.Č. was funded by a Scientific Grant Agency of the Ministry of Education of Slovak Republic and Slovak Academy of Sciences (grant number 1/0191/21). Comparative CT scans of squamates were obtained from the Collaborative Research: oVert: Open Exploration of Vertebrate Diversity in 3D funded by National Science Foundation (DBI 1701714). Amber scanning, travel grants, and scientific illustration were sponsored by the Peretti Foundation. We thank Thomas L. Stubbs for his help in calculating Cramér coefficients and for sharing the relevant R script. Special thanks to Stephanie Abramowicz for the reconstruction of *Oculudentavis* and to Monica Solórzano and Enrique Peñalver for assistance identifying the flies associated with the specimen.

AUTHOR CONTRIBUTIONS

Conceptualization, S.E.E., A.B., A.P., E.L.S., J.D.D., A.Č., and A.M.B.; methodology, A.B., E.L.S., J.D.D., J.S.A., M.V.-G., J.J.B., and A.P.; investigation, A.B., E.L.S., J.D.D., J.S.A., A.Č., M.V.-G., A.M.B., J.J.B., S.E.E., and A.P.; writing – original draft, S.E.E.; writing – review & editing, A.B., E.L.S., J.D.D., J.S.A., A.Č., M.V.-G., A.M.B., J.J.B., A.P., and S.E.E.; resources, A.B., E.L.S., J.D.D., J.J.B., and A.P.; supervision, A.B., J.D.D., S.E.E., and J.J.B.

DECLARATION OF INTERESTS

The authors declare no competing interests.

Received: August 20, 2020
Revised: March 22, 2021
Accepted: May 18, 2021
Published: June 14, 2021

REFERENCES

1. Xing, L., O'Connor, J.K., Schmitz, L., Chiappe, L.M., McKellar, R.C., Yi, Q., et al. (2020). Hummingbird-sized dinosaur from the Cretaceous period of Myanmar. Nature *579*, 245–249.
2. Atterholt, J., Hutchison, J.H., and O'Connor, J.K. (2018). The most complete enantiornithine from North America and a phylogenetic analysis of the Avisauridae. PeerJ *6*, e5910.
3. Li, Z.-H., Wang, W., Hu, H., Wang, M., Yi, H., and Lu, J. (2020). Reanalysis of *Oculudentavis* shows it is a lizard. Vertebrat. PalAsiatic. Published online August 17, 2020. https://doi.org/10.19615/j.cnki.1000-3118.201020.
4. Pritchard, A.C., and Sues, H.-D. (2019). Postcranial remains of *Teraterpeton hrynewichorum* (Reptilia: Archosauromorpha) and the mosaic evolution of the saurian postcranial skeleton. J. Syst. Palaeontology *17*, 1745–1765.
5. O'Connor, J., Xing, L., Chiappe, L., Schmitz, L., Li, G., and Yi, Q. (2020). Reply to Li et al. "Is *Oculudentavis* a bird or even archosaur?". bioRxiv. https://doi.org/10.1101/2020.06.12.147041.

6. Pritchard, A.C., and Nesbitt, S.J. (2017). A bird-like skull in a Triassic diapsid reptile increases heterogeneity of the morphological and phylogenetic radiation of Diapsida. R. Soc. Open Sci. *4*, 170499.
7. Gauthier, J.A., Kearney, M., Maisano, J.A., Rieppel, O., and Behlke, A.D.B. (2012). Assembling the squamate tree of life: perspectives from the phenotype and the fossil record. Bull. Peabody Mus. Nat. Hist. *53*, 3–308.
8. Xing, L., O'Connor, J.K., Schmitz, L., Chiappe, L.M., McKellar, R.C., Yi, Q., and Li, G. (2020). Retraction note: Hummingbird-sized dinosaur from the Cretaceous period of Myanmar. Nature *584*, 652.
9. Dubois, A. (2020). 'Retraction' of taxonomic papers: the meaning of the word 'issued' and related ones in zoological nomenclature. Zoosystema *42*, 519–523.
10. Dubois, A. (2020). Nomenclatural consequences of the *Oculudentavis khaungraae* case, with comments on the practice of 'retraction' of scientific publications. Zoosystema *42*, 475–482.
11. Krell, F.-T. (2015). A mixed bag: when are early online publications available for nomenclatural purposes? Bull. Zool. Nomenclat. *72*, 19–32.
12. Vlachos, E. (2020). A response to Dubois (2020; Zoosystema 42 (23): 475-482). Zoosystema *42*, 475–482.
13. Gauthier, J., Kluge, A.G., and Rowe, T. (1988). Amniote phylogeny and the importance of fossils. Cladistics *4*, 105–209.
14. Shi, G., Grimaldi, D.A., Harlow, G.E., Wang, J., Wang, J., Yang, M., Lei, W., Li, Q., and Li, X. (2012). Age constraint on Burmese amber based on U–Pb dating of zircons. Cretac. Res. *37*, 155–163.
15. Zheng, Y., and Wiens, J.J. (2016). Combining phylogenomic and supermatrix approaches, and a time-calibrated phylogeny for squamate reptiles (lizards and snakes) based on 52 genes and 4162 species. Mol. Phylogenet. Evol. *94* (Pt B), 537–547.
16. Sanger, T.J., Sherratt, E., McGlothlin, J.W., Brodie, E.D., 3rd, Losos, J.B., and Abzhanov, A. (2013). Convergent evolution of sexual dimorphism in skull shape using distinct developmental strategies. Evolution *67*, 2180–2193.
17. Dutchak, A.R., and Caldwell, M.W. (2009). A redescription of *Aigialosaurus* (= *Opetiosaurus*) Bucchichi (Kornhuber, 1901) (Squamata: Aigialosauridae) with comments on Mosasauroid systematics. J. Vertebr. Paleontol. *29*, 437–452.
18. Paparella, I., Palci, A., Nicosia, U., and Caldwell, M.W. (2018). A new fossil marine lizard with soft tissues from the Late Cretaceous of southern Italy. R. Soc. Open Sci. *5*, 172411.
19. Schmitz, L., and Motani, R. (2010). Morphological differences between the eyeballs of nocturnal and diurnal amniotes revisited from optical perspectives of visual environments. Vision Res. *50*, 936–946.
20. Schmitz, L., and Motani, R. (2011). Nocturnality in dinosaurs inferred from scleral ring and orbit morphology. Science *332*, 705–708.
21. Stayton, C.T. (2006). Testing hypotheses of convergence with multivariate data: morphological and functional convergence among herbivorous lizards. Evolution *60*, 824–841.
22. Volume Graphics (2020). VGSTUDIO MAX, high-end industrial CT software. https://www.volumegraphics.com/en/products/vgstudio-max.html.
23. Goloboff, P., and Catalano, S.A. (2016). TNT version 1.5, including a full implementation of phylogenetic morphometrics. Cladistics *32*, 221–238.
24. Lloyd, G.T. (2016). Estimating morphological diversity and tempo with discrete character-taxon matrices: implementation, challenges, progress, and future directions. Biol. J. Linn. Soc. Lond. *118*, 131–151.
25. R Development Core Team (2019). R: A language and environment for statistical computing (R Foundation for Statistical Computing).
26. Bapst, D.W. (2012). paleotree: an R package for paleontological and phylogenetic analyses of evolution. Methods Ecol. Evol. *3*, 803–807.
27. Sievert, C. (2018). Plotly for R v. 4.9.0. https://pypi.org/project/plotly/.
28. Adams, D., Collyer, M., and Kaliontzopoulou, A. (2020). Geomorph: Geometric Morphometric Analyses of 2D/3D Landmark Data, v. 3.2.1. https://github.com/geomorphR/geomorph.
29. Schlager, S. (2017). Morpho and Rvcg - shape analysis in R. In Statistical Shape and Deformation Analysis, G. Zheng, S. Li, and G. Szekely, eds. (Academic), pp. 217–256.
30. Stratovan Corporation (2018). Stratovan Checkpoint. Version 2018.08.07. https://www.stratovan.com/products/checkpoint.
31. Rayfield, E.J., Theodor, J.M., and Polly, P.D. (2020). Fossils from conflict zones and reproducibility of fossil-based scientific data. http://vertpaleo.org/GlobalPDFS/SVP-Letter-to-Editors-FINAL.aspx.
32. Rayfield, E.J., Theodor, J.M., and Polly, P.D. (2020). Further Information on Myanmar amber, mining, human rights violations, and amber trade. http://vertpaleo.org/Society-News/SVP-Paleo-News/Society-News,-Press-Releases/Further-information-on-Myanmar-amber,-mining,-huma.aspx.
33. Musa, M., Kaye, T.G., Bieri, W., and Peretti, A. (2021). Burmese amber compared using micro-attenuated total reflection infrared spectroscopy and ultraviolet imaging. Appl. Spectrosc. Published online January 21, 2021. https://doi.org/10.1177/0003702820986880.
34. Paganin, D., Mayo, S.C., Gureyev, T.E., Miller, P.R., and Wilkins, S.W. (2002). Simultaneous phase and amplitude extraction from a single defocused image of a homogeneous object. J. Microsc. *206*, 33–40.
35. Gureyev, T.E., Nesterets, Y., Ternovski, D., Thompson, D., Wilkins, S.W., Stevenson, A.W., Sakellariou, A., and Taylor, J.A. (2011). Toolbox for advanced X-ray image processing. In Proceedings Volume 8141, Advances in Computational Methods for X-Ray Optics II (SPIE), p. 81410B.
36. Goloboff, P.A. (1999). Analyzing large data sets in reasonable times: solutions for composite optima. Cladistics *15*, 415–428.
37. Nixon, K.C. (1999). The parsimony ratchet, a new method for rapid parsimony analysis. Cladistics *15*, 407–414.
38. Goloboff, P.A. (1993). Estimating character weights during tree search. Cladistics *9*, 83–91.
39. Goloboff, P.A., Carpenter, J.M., Arias, J.S., and Mirande Esquivel, D.R. (2008). Weighting against homoplasy improves phylogenetic analysis of morphological data sets. Cladistics *24*, 758–773.
40. Goloboff, P.A., Torres, A., and Arias, J.S. (2018). Weighted parsimony outperforms other methods of phylogenetic inference under models appropriate for morphology. Cladistics *34*, 407–437.
41. Kotrc, B., and Knoll, A.H. (2015). A morphospace of planktonic marine diatoms. I. Two views of disparity through time. Paleobiology *41*, 45–67.
42. Nordén, K.K., Stubbs, T.L., Prieto-Márquez, A., and Benton, M.J. (2018). Multifaceted disparity approach reveals dinosaur herbivory flourished before the end-Cretaceous mass extinction. Paleobiology *44*, 620–637.
43. Schlager, S., Profico, A., Di Vincenzo, F., and Manzi, G. (2018). Retrodeformation of fossil specimens based on 3D bilateral semi-landmarks: implementation in the R package "Morpho". PLoS ONE *13*, e0194073.
44. Vidal-García, M., Bandara, L., and Keogh, J.S. (2018). ShapeRotator: An R tool for standardized rigid rotations of articulated three-dimensional structures with application for geometric morphometrics. Ecol. Evol. *8*, 4669–4675.
45. Vidal-García, M., Bandara, L., and Keogh, J.S. (2020). ShapeRotator: standarised rigid rotations of articulated three-dimensional structures. R package version 0.1.0. https://CRAN.R-project.org/package=ShapeRotator.
46. Bookstein, F.L. (1989). Principal warps: thin-plate splines and the decomposition of deformations. IEEE Trans. Pattern Anal. Mach. Intell. *11*, 567–585.

Please cite this article in press as: Bolet et al., Unusual morphology in the mid-Cretaceous lizard *Oculudentavis*, Current Biology (2021), https://doi.org/10.1016/j.cub.2021.05.040

CellPress
OPEN ACCESS

STAR★METHODS

KEY RESOURCES TABLE

REAGENT or RESOURCE	SOURCE	IDENTIFIER
Deposited data		
Raw HRCT data	This paper	https://www.morphosource.org/media/000165457
3D model of *Oculudentavis khaungraae*	This paper	https://tinyurl.com/Oculudentavis-A-10420
3D model of *Oculudentavis naga*	This paper	https://tinyurl.com/Oculudentavis-L-10420
Phylogenetic matrices	This paper	http://morphobank.org/permalink/?P4028
Software and algorithms		
VGSTUDIO MAX	Volume Graphics[22]	https://www.volumegraphics.com
TNT v1.1	Goloboff and Catalano[23]	http://www.lillo.org.ar/phylogeny/tnt/
Claddis package v. 0.2.0	Lloyd[24]	https://cran.r-project.org/web/packages/Claddis/index.html
R	R Development Core Team[25]	https://cran.r-project.org/mirrors.html
package paleotree v. 3.3.0	Bapst[26]	https://github.com/dwbapst/paleotree
package Plotly v. 4.9.0	Sievert[27]	https://pypi.org/project/plotly/
Geomorph v. 3.1.0	Adams et al.[28]	https://github.com/geomorphR/geomorph
Morpho	Schlager[29]	N/A
Stratovan Checkpoint	Stratovan Corporation[30]	https://www.stratovan.com/products/checkpoint
Retrodeformation code\	This paper	https://github.com/marta-vidalgarcia/Oculudentavis_retrodeformation

RESOURCE AVAILABILITY

Lead contact

Further information and requests for resources should be directed to and will be fulfilled by the lead contact, Juan D. Daza (juand.daza@gmail.com).

Materials availability

The holotype of *Oculudentavis naga* (GRS-Ref-28627) is housed at the Peretti Museum Foundation in Meggen, Switzerland.

The holotype of *Oculudentavis khaungraae* (BP/1/7120) is housed at the Hupoge Amber Museum in Tengchong, China.

Data and code availability

The download links to the 3D models of *Oculudentavis khaungraae* and *Oculudentavis naga* are https://tinyurl.com/Oculudentavis-A-10420 and https://tinyurl.com/Oculudentavis-L-10420, respectively.

The retrodeformation code is available at https://github.com/marta-vidalgarcia/Oculudentavis_retrodeformation. Phylogenetic data sets are available at http://morphobank.org/permalink/?P4028

EXPERIMENTAL MODEL AND SUBJECT DETAILS

Ethics statement

As researchers working on amber fossil inclusions, we follow the recommendations sent by the officers of the Society for Vertebrate Paleontology (SVP) to many editors of scientific journals.[31,32] Many of us are members of SVP, and we acknowledge their concerns as to the origin of Burmese amber material from conflict zone areas in Myanmar, human rights violations caused by its inappropriate commercialization, and the worry that some private fossil collectors are exploiting the commercial value of these fossils without considering the long-term accessibility of this material to the scientific community.

The holotype specimen of *Oculudentavis naga* (GRS-Ref-28627) and the holotype of *O. khaungraae* (HPG-15-3) were recovered from the same mine (Aung Bar mine, 26° 09′ N, 96° 34′ E). Both specimens were recovered prior to the conflict in late 2017 (Supplemental information). GRS-Ref-28627 was presented to one of the authors of this paper (AP) by local intermediaries for inspection during a humanitarian mission to the Tanai area, led by GemResearch Swiss Laboratory (GRS).

The holotype specimen of *Oculudentavis naga* was acquired from an authorized company that exports amber pieces legally outside of Myanmar, following an ethical code that assures no violations of human rights were committed in the process of mining, and commercialization. The referred specimen was initially loaned on consignment to GRS during a Bangkok show in 2018, for chemical, physical and spectroscopic analysis. Following these tests, the specimen was returned to Myanmar by the Myanmarese owner, and exported through a jewelry show in Yangon officially through a broker of GRS, whereupon it passed through definitive official export channels, and subsequently entered the GRS collection in Switzerland. AP strongly affirms that no funds from the sale of this amber specimen have been directed to support conflict in Kachin. A movie of the mine visit is available upon request from AP. The Peretti Museum Foundation is an officially established, not-for-profit organization, founded in Switzerland by the Peretti family. The Museum promises ethical compliance in connection with the acquisition of material and supports charity projects in mining areas. The Museum actively supports research and knowledge, and provides a framework for expert collaboration and public access to all type specimens and associated content for study and publication in academic literature and other outlets. The special legal structure of the non-profit Peretti Museum Foundation law mandatorily guarantees under Swiss law that inventory of the foundation with GRS Reference numbers can never be lost to science. A description and further details regarding the timing and a discussion of the military escalation in the Tanai area, and details regarding the ethical acquisition of amber pieces from Myanmar are available at the Museum website: https://www.pmf.org. The referred specimen has an authenticated paper trail, including export permits from Myanmar. All documentation relevant to the acquisition of the holotype specimen of *Oculudentavis naga* is available in the Supplemental information section. Detail information of the ethical acquisition of amber pieces can be found in the following link: https://372fddf1-abf8-4bcf-897d-e5819bb34d6e.filesusr.com/ugd/31bd21_fb8d0e5bcbe34ff0bb8294a260a21670.pdf.

METHOD DETAILS

Spectroscopy and stratigraphic data

Fourier-transform infrared (FTIR) spectrum data of the specimen was recorded and compared to a number of reference specimens extracted directly from the Aung Bar mine by GRS staff, and to FTIR spectra of specimens obtained from other mines and localities across Myanmar. Likewise, the inclusion pattern (banding with bubble flows, etc.) was compared to other self-collected (by A.P) Aung Bar materials. FTIR matrix and inclusion analyses conclusively verify the indicated origin of the material from the Aung Bar mine.[33]

GRS representatives visited the mine shaft from which the specimen was recovered, and a GoPro recording was made of the trip down the mine to the approximate location from which the specimen was found within the 1-2-m-thick amber-containing rock layer. A miner was commissioned to recover a sample with GoPro recording of this amber-bearing rock for archiving and further analysis. Stratigraphic analysis of the entire mine column is yet to be conducted.

Synchrotron Scanning

Microtomographic measurements of *Oculudentavis naga* were performed using the Imaging and Medical Beamline (IMBL) at the Australian Nuclear Science and Technology Organization's (ANSTO) Australian Synchrotron, Melbourne, Australia. For this investigation, acquisition parameters included a pixel size of 5.8 × 5.8 μm, monochromatic beam energy of 28 keV, a sample-to-detector distance of 100 cm and use of the "Ruby" detector consisting of a PCO.edge sCMOS camera (16-bit, 2560 × 2160 pixels) and a Nikon Makro Planar 100 mm lens coupled with a 20 μm thick Gadox/CsI(Tl)/$CdWO_4$ scintillator screen. As the height of the specimen exceeded the detector field-of-view, the specimen was aligned axially relative to the beam and imaged using three consecutive scans, each consisting of 1800 equally-spaced angle shadow-radiographs with an exposure length of 0.50 s, obtained every 0.10° as the sample was continuously rotated 180° about its vertical axis. Vertical translation of the specimen between tomographic scans was 11 mm. 100 dark (closed shutter) and beam profile (open shutter) images were obtained for calibration before and after shadow-radiograph acquisition. Total time for the scan was 52 min.

The raw 16-bit radiographic series were normalized relative to the beam calibration files and combined using IMBL Stitch software to yield a 32-bit series with a field-of-view of 14.8 × 29.4 mm. Reconstruction of the 3-D dataset was achieved by the filtered-back projection method and TIE-Hom algorithm phase retrieval[34] using the CSIRO's X-TRACT.[35] The reconstructed volume data were rendered and visualized using VGStudio Max.[22]

Phylogenetic analysis

The two specimens assigned to *Oculudentavis* were retrofitted into a character matrix for squamates, including phenotypic[7] and molecular data.[15] We were able to score 374 characters in *Oculudentavis naga* (GRS-Ref-28627; 61.3% scored), but only 302 in *O. khaungraae* (HPG-15-3; 49.5% scored). The character scores that were available on both specimens are very similar, although part of the large amount of missing data in *O. khaungraae* is due to the preservation of the specimen that makes it difficult to follow suture lines. Fifteen characters have different scores for *O. khaungraae* and *O. naga* (see the detailed list in the Supplemental Information). All analyses were performed with TNT.[23] We searched for the best tree over all matrices with equal weights, treating characters as either ordered (Figure 5C; Data S1, Combined evidence tree for squamate dataset using the ordered scheme) or unordered (Figure 5D; Data S1, Combined evidence tree for squamate dataset using the unordered scheme). An additional search was run on a version of the dataset that included just the morphological characters (Figure 5E; Data S1, Morphological tree for squamate dataset using the ordered scheme). On each run we used a script to search with new technologies (*xmult* command), starting with 20 trees of random addition, using exclusive and random sectorial searches,[36] as well as 25 rounds of ratchet[37] and tree drift,[36] and fusing trees

Please cite this article in press as: Bolet et al., Unusual morphology in the mid-Cretaceous lizard *Oculudentavis*, Current Biology (2021), https://doi.org/10.1016/j.cub.2021.05.040

every five rounds. This procedure was repeated until 20 independent hits of minimal length were found. All the best trees, as well as the strict consensus were stored. To calculate node support, we use a TBR swapping option as implemented in TNT to calculate Bremmer support values holding trees up to 10 steps beyond the optimal tree (*bsupp* command). Wildcards were detected using the *prunnel* command; wildcard terminals were removed from optimal trees found with all terminals activated, and the consensus was calculated from that resulting pruned trees (i.e., character scores from wildcard terminals were considered).

The two specimens of *Oculudentavis* were also coded into a general amniote data matrix[6] to test their position in relation to both birds (represented by *Archaeopteryx*, *Confuciusornis, Columba*), and squamates. We also added the non-avian theropod *Velociraptor mongoliensis* and the crocodylomorph *Crocodylus acutus*. We were able to score 151 characters for *Oculudentavis naga* (49.2% scored), and 108 of *O. khaungraae* (35.1% scored). We searched for the best tree using implied weights,[38–40] increasing the concavity value using a size of class interval of 10 from 10 to 200. As the size of the matrix is average, we used TNT[23] with a traditional search with 200 trees of random addition (*mult* command). The reported tree corresponds to the single topology recovered under the different values of concavity (Figure 5A). To test the cost of forcing *Oculudentavis* as a bird, we ran a search with equal weights in implied weights constraining *Oculudentavis* as a bird, but without any defined location and compared its length with an unconstrained tree.

Phylomorphospace analysis

The phylomorphospace provides the position of taxa in a bidimensional (Data S1, 2D Phylomorphospace using the amniotes matrix) or tridimensional (Data S1, 3D Phylomorphospace using the amniote matrix) morphospace distributed according to the values of the distance matrix, with the morphological matrix as the source. All nodes and tips are connected by lines that represent the branches in the phylogeny. One advantage of phylomorphospace plots is that they make it easier to recognize whether clades and/or ecological groups plot in distinct areas of morphospace.

Phylomorphospace analyses using the morphological character matrices were run in Claddis package v. 0.2.0[24] in R.[25] One phylogeny resulting from each dataset was selected to be used in plotting phylomorphospaces. They were dated using the "equal" method of the timePaleoPhy function in the package paleotree v. 3.3.0.[26] The package Plotly v. 4.9.0[27] was used to generate an interactive plot of 3D morphospace. The package Geomorph v. 3.1.0[28] was used to generate an interactive plot of 3D phylomorphospace, of which reported figures (Data S1) are (modified) screenshots. The strength of association between characters and PCO axes was calculated using Cramér coefficients (see Kotrc and Knoll[41]) as adapted in Nordén et al.,[42] see Data S1, Cramér coefficients and p values.

Retrodeformation analysis

The rendered volume data for the two *Oculudentavis* species was exported as three-dimensional (3D) surface meshes using VGStudio Max.[22] A dense set of landmarks (containing landmarks, curve-semilandmarks, and 3D surface semilandmarks, see Data S1, Distribution of 3D landmarks used in the retrodeformation) was placed across multiple regions in the 3D surface meshes to capture detailed overall skull shape in each specimen, using Stratovan Checkpoint,[30] before being exported as CSV files for further analyses.

Despite multiple similarities in osteological features between the two specimens assigned to *Oculudentavis*, there are some overall skull shape differences that could be easily attributable to deformations caused by taphonomic processes. Even though recently developed analytical methods can virtually retrodeform fossil specimens, this has only been developed for taphonomically-induced bilateral asymmetry.[43] Here we present a virtual retrodeformation workflow for dorso-ventrally taphonomic deformations based on 3D landmark data, using the open-source software R.[25]

Landmark data and 3D surface meshes were imported into R using the file2mesh function in Morpho.[29] We used the R package ShapeRotator[44,45] to place both skulls on the x,z plane, thereby facilitating all subsequent retrodeformation operations. Since each *Oculudentavis* specimen exhibited deformations in different regions of the cranium, identified by asymmetries, distortions, and bone displacements, we performed different retrodeformation operations on each specimen.

For the *Oculudentavis khaungraae* specimen, we identified the premaxilla, maxilla and dentary as the points showing the maximum effects of taphonomic deformation that contributed to its bird-like appearance, both laterally and dorso-ventrally. We first addressed the lateral compression of the rostrum by increasing the distance between the landmark sets on the premaxilla, maxillae and the skull's lateral midline. We then addressed the dorso-ventral compression on the x,y plane, mostly affecting the nasal crest, premaxilla, and maxillae.

For *Oculudentavis naga*, we identified a dorso-ventral compression of the vault. We first retrodeformed the orbits on the x,y plane to a more 'natural' ellipsoid shape, as they had been highly affected by dorso-ventral compression. After obtaining a model with the most likely orbit shape (as determined by the shape and proportions of the ring of scleral ossicles), we proceeded to model the deformation effects on the nasals, prefrontals, frontals, and postfrontals. Finally, the supraoccipital was retrodeformed to be oriented in a more vertical position than preserved, to reconstruct an accurate vault shape, as this region had been taphonomically deformed and displaced at an angle relative to the rest of the vault.

After obtaining the retrodeformation models for both specimens, we used a thin-plate spline method[46] to interpolate surface changes from the 3D landmark data onto the 3D surface mesh, using the R function tps3d in Morpho. We visualized shape variation between the original and retrodeformed 3D surface meshes by plotting heatmaps onto the retrodeformed meshes, using the function meshDist in Morpho.[29] These heatmaps indicate the degree of deformation in different regions of the skulls, with yellow and dark blue representing no deformation and high deformation respectively.

Current Biology, Volume *31*

Supplemental Information

Unusual morphology in the mid-Cretaceous lizard *Oculudentavis*

Arnau Bolet, Edward L. Stanley, Juan D. Daza, J. Salvador Arias, Andrej Čerňanský, Marta Vidal-García, Aaron M. Bauer, Joseph J. Bevitt, Adolf Peretti, and Susan E. Evans

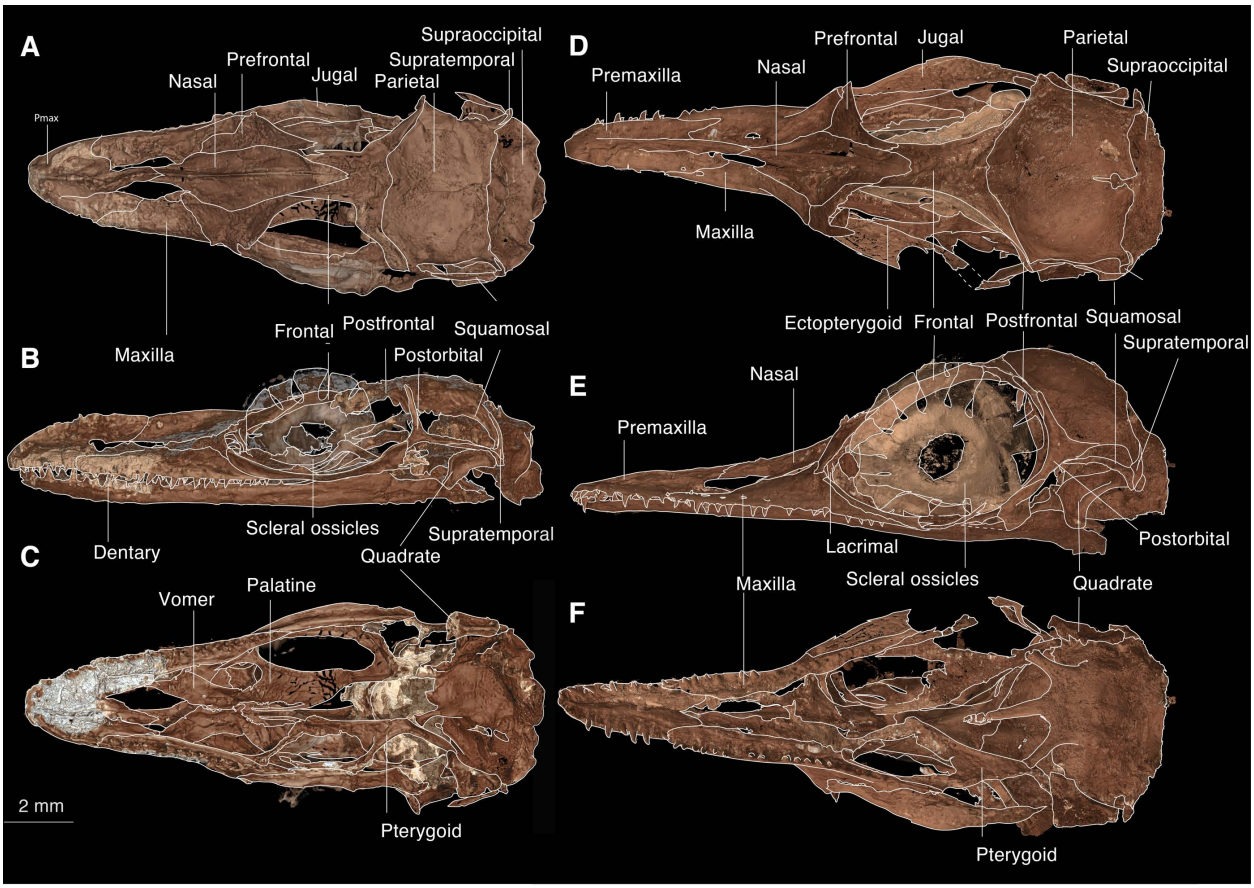

Figure S1. Articulated skulls of *Oculudentavis* species with bone interpretation based on the digital segmentation. Related to Figures 1, 2. A–C, *O. naga*, D–K, *O. khaungraae*. Scale bar equals 2 mm.

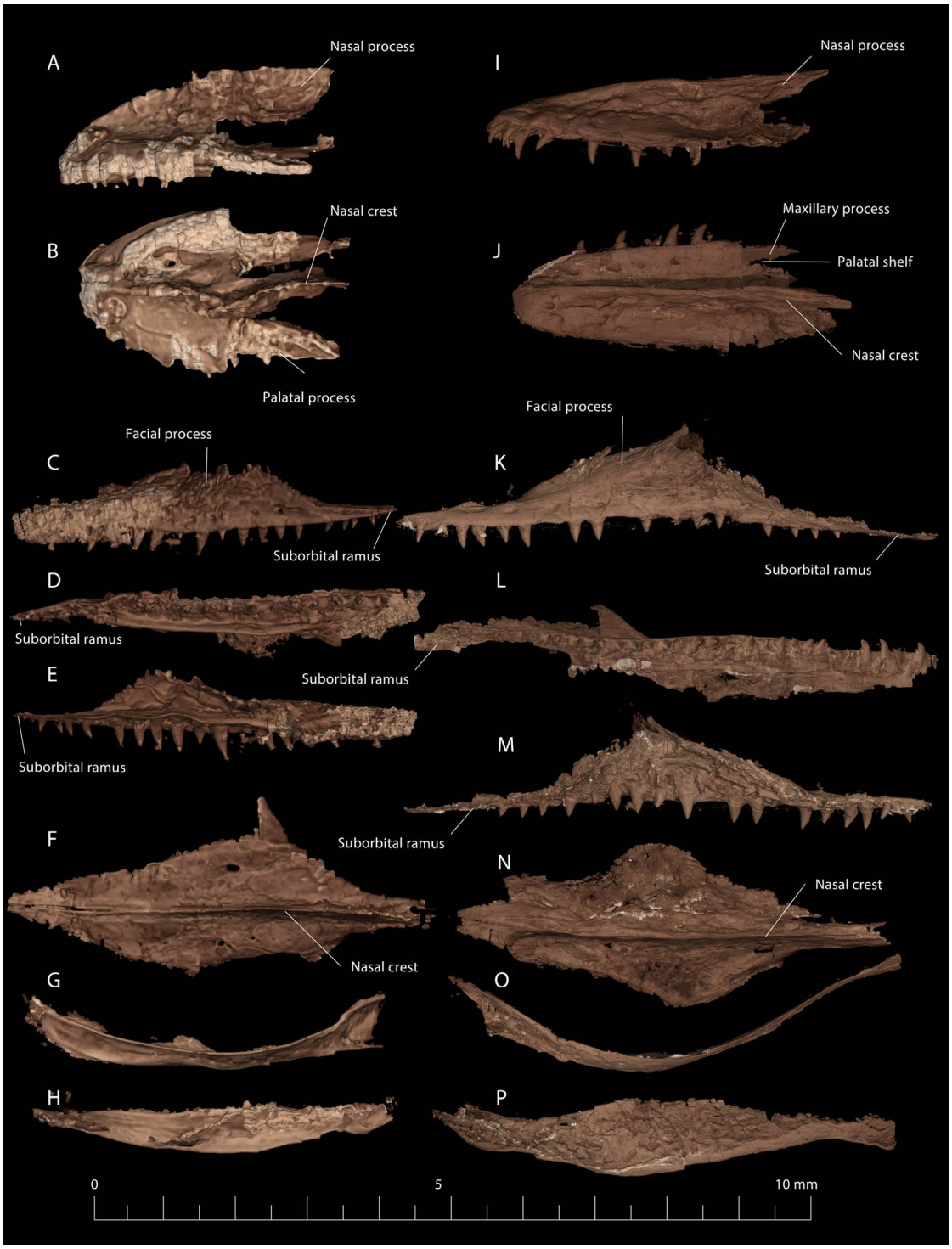

Figure S2. Segmented skull elements. Related to Figures 1, 2. A–H, *Oculudentavis naga*; I–P, *O. khaungraae*. Lateral view of the premaxilla (A, I); dorsal view of the premaxilla (B, J). Left maxilla in lateral (C, K), occlusal (D, L), and medial (E, M) views. Nasals in dorsal view (F, N), and right jugal bones in lateral (G, O) and dorsal views (H, P).

Figure S3. Segmented skull elements. Related to Figures 1, 2. A–D, *Oculudentavis naga*; E–H, *O. khaungraae*. Dorsal view of the frontal and nasal (A, E); dorsal view of the parietal (B, F); lateral view of the left (C), and right (G) postorbitals, and lateral views of the left squamosal (D, H).

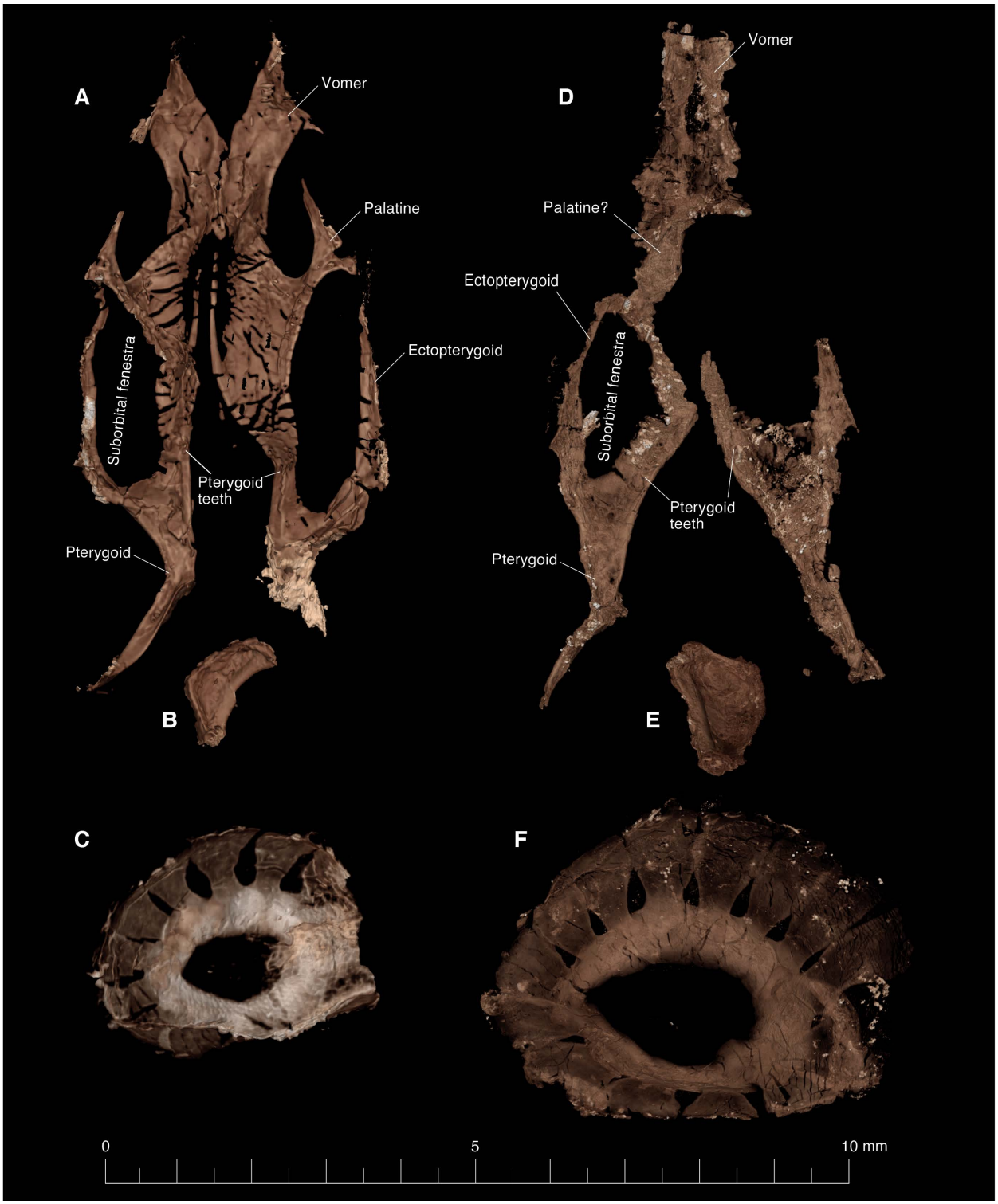

Figure S4. Segmented skull elements. Related to Figures 1, 2. A–C, *Oculudentavis naga*; D–F, *O. khaungraae*. Ventral view of the palatal bones (A, D); left quadrate (B); right quadrate (E); left scleral ossicle series (C, F). Related to Figures 1, 2.

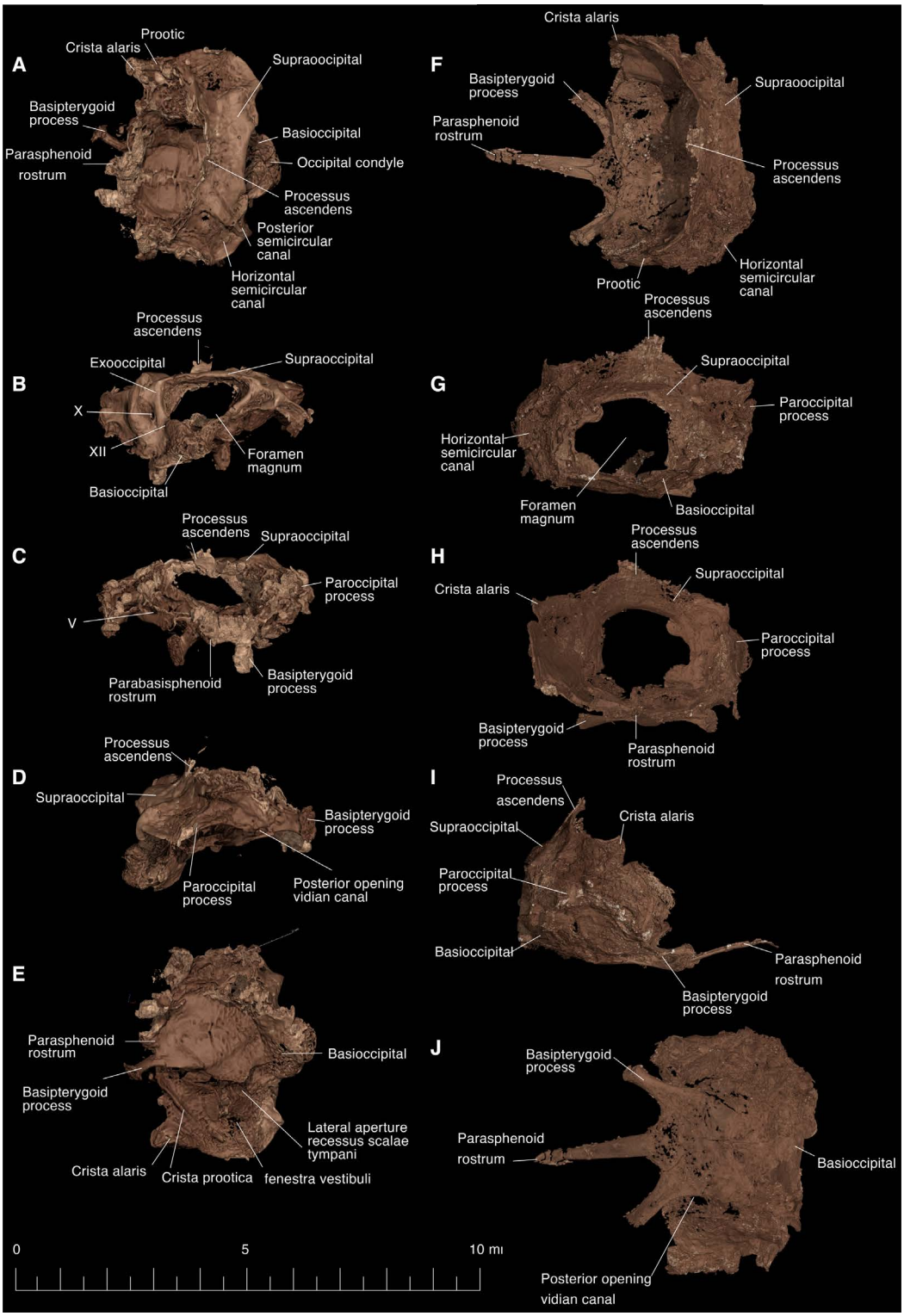

Figure S5. Segmented braincase. Related to Figures 1, 2. *Oculudentavis naga* (A–E), *O. khaungraae* (F–J). Dorsal (A, F), posterior (B, G), anterior (C, H), lateral right side (D, I), and ventral (E, J) views.

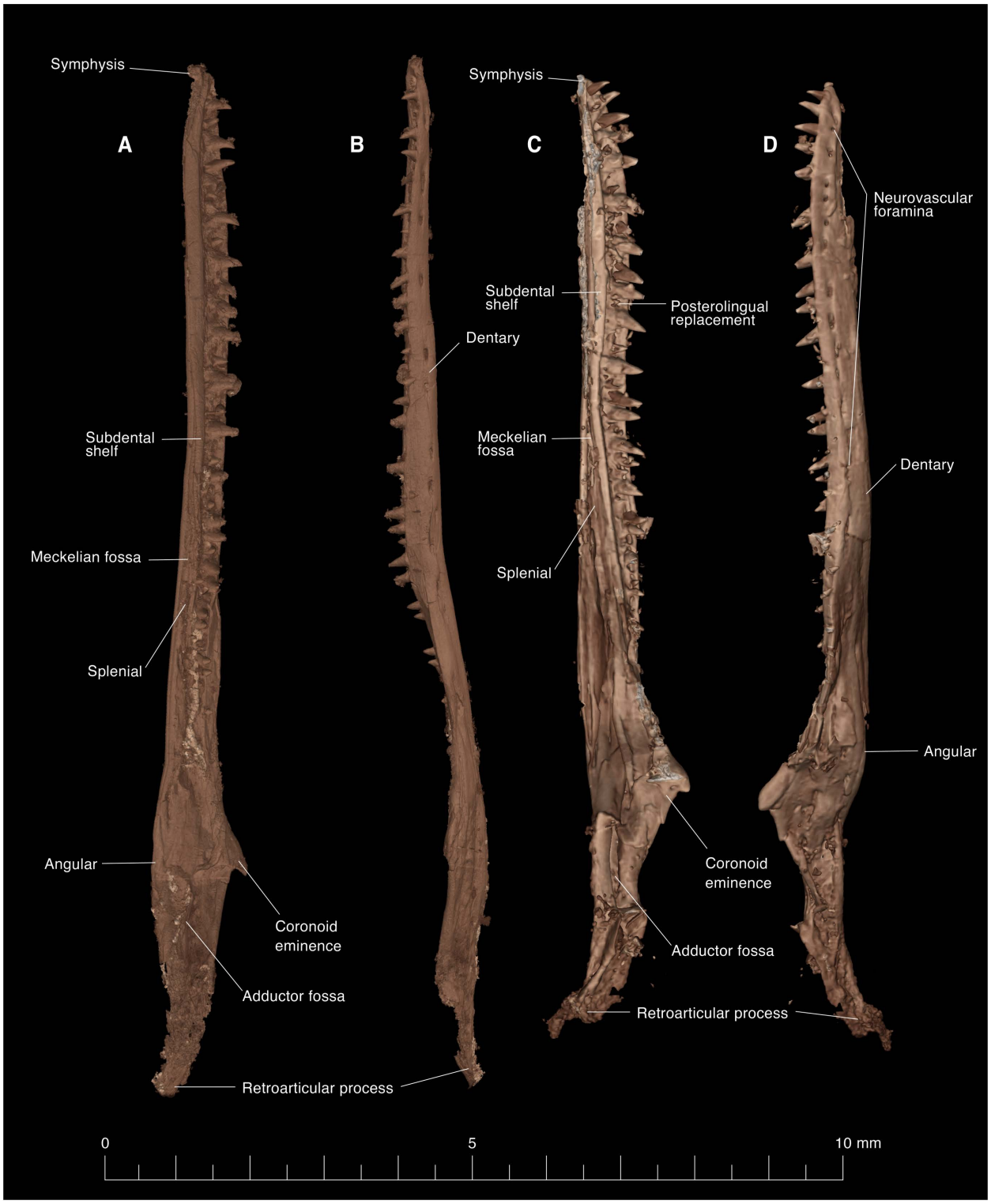

Figure S6. Segmented jaws. Related to Figures 1, 2. *Oculudentavis naga* (A–B), *O. khaungraae* (C–D). Lingual (A, C) and labial (B, D) views of the right ramus.

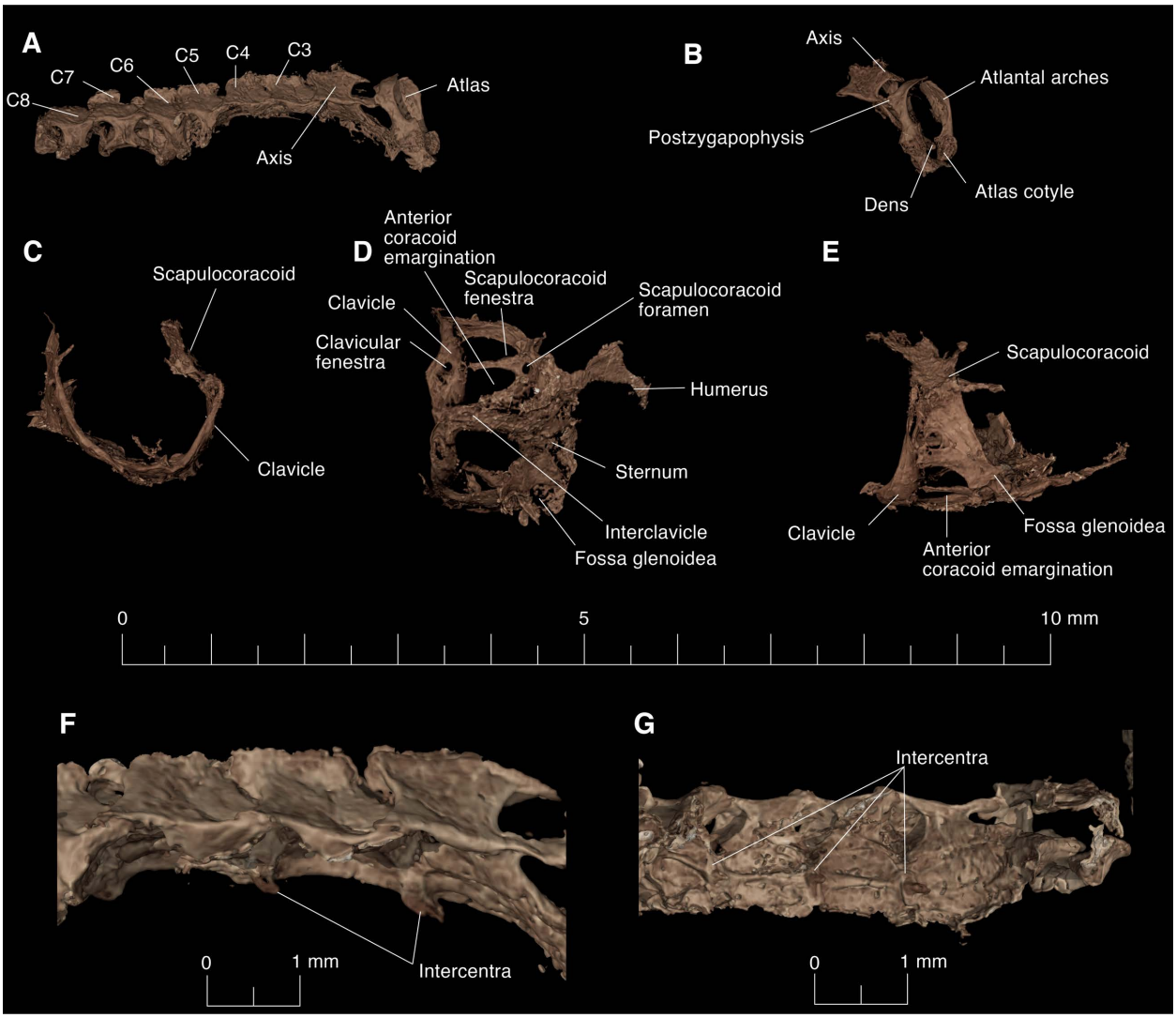

Figure S7. Postcranial elements of *Oculudentavis naga*. Related to Figures 1, 2.

Cervical vertebrae, right lateral view of cervical column (A) and right lateral view of atlas-axis (B), pectoral girdle (C–E), close up of the cervical column showing the intercentra in left lateral (F), and ventral (G) views.

Supplemental References

S1. Pritchard, A.C., and Nesbitt, S.J. (2017). A bird-like skull in a Triassic diapsid reptile increases heterogeneity of the morphological and phylogenetic radiation of Diapsida. Roy Soc Open Sci *4*.

S2. Gauthier, J., Kearney, M., Maisano, J.A., Rieppel, O., and Behlke, A. (2012). Assembling the squamate tree of life: perspectives from the phenotype and the fossil record. Bull. Peabody Mus. Nat. Hist. *53*, 3–308

S3. Zheng, Y.C., and Wiens, J.J. (2016). Combining phylogenomic and supermatrix approaches, and a time-calibrated phylogeny for squamate reptiles (lizards and snakes) based on 52 genes and 4162 species. Mol. Phylogenet. Evol. *94*, 537–547.